HHS Public Access

Author manuscript

Arterioscler Thromb Vasc Biol. Author manuscript; available in PMC 2023 April 01.

Published in final edited form as:

Arterioscler Thromb Vasc Biol. 2022 April ; 42(4): 407–427. doi:10.1161/ATVBAHA.121.317182.

Novel role of pre-replication complex component cell division cycle 6 in retinal neovascularization

Raj Kumar, **Gadiparthi N. Rao**

Department of Physiology, University of Tennessee Health Science Center, Memphis, TN 38163, USA

Abstract

Background: The major aim of this study is to investigate whether cell division cycle 6 (CDC6), a replication origin recognition complex component, plays a role in retinal neovascularization, and if so, to explore the underlying mechansims.

Methods: In this study, we used a variety of approaches including cellular and moleculer biological methodologies as well as global and tissue-specific knockout mice in combination with an oxygen-induced retinopathy (OIR) model to study the role of CDC6 in retinal neovascularization.

Results: Vascular endothelial growth factor A (VEGFA) induced CDC6 expression in a time-dependent manner in human retinal microvascular endothelial cells (HRMVECs). In addition, VEGFA-induced CDC6 expression was dependent on phospholipase Cβ3 (PLCβ3)-mediated nuclear factor of activated T cells c1 (NFATc1) activation. Furthermore, while siRNA-mediated depletion of PLCβ3, NFATc1, or CDC6 levels blunted VEGFA-induced HRMVEC angiogenic events such as proliferation, migration, sprouting, and tube formation, CDC6 overexpression rescued these effects in NFATc1-deficient mouse retinal microvascular endothelial cells. In accordance with these observations, global knockdown of PLCβ3 or endothelial cell (EC)-specific deletion of NFATc1 or siRNA-mediated depletion of CDC6 levels substantially inhibited OIR-induced retinal sprouting and neovascularization. In addition, retroviral-mediated overexpression of CDC6 rescued OIR-induced retinal neovascularization from inhibition in PLCβ3 knockout mice and in EC-specific NFATc1-deficient mice.

Conclusions: The above observations clearly reveal that PLCβ3-mediated NFATc1 activation-dependent CDC6 expression plays a crucial role in VEGFA/OIR-induced retinal neovascularization.

Graphical Abstract

Address for correspondence Gadiparthi N. Rao, Ph.D. Department of Physiology, 71 S Manassas Street, TSRB, Rm 310J, University of Tennessee Health Science Center, Memphis, TN 38163, USA, Phone: 901-448-7321, rgadipar@uthsc.edu.

DISCLOSURES

None

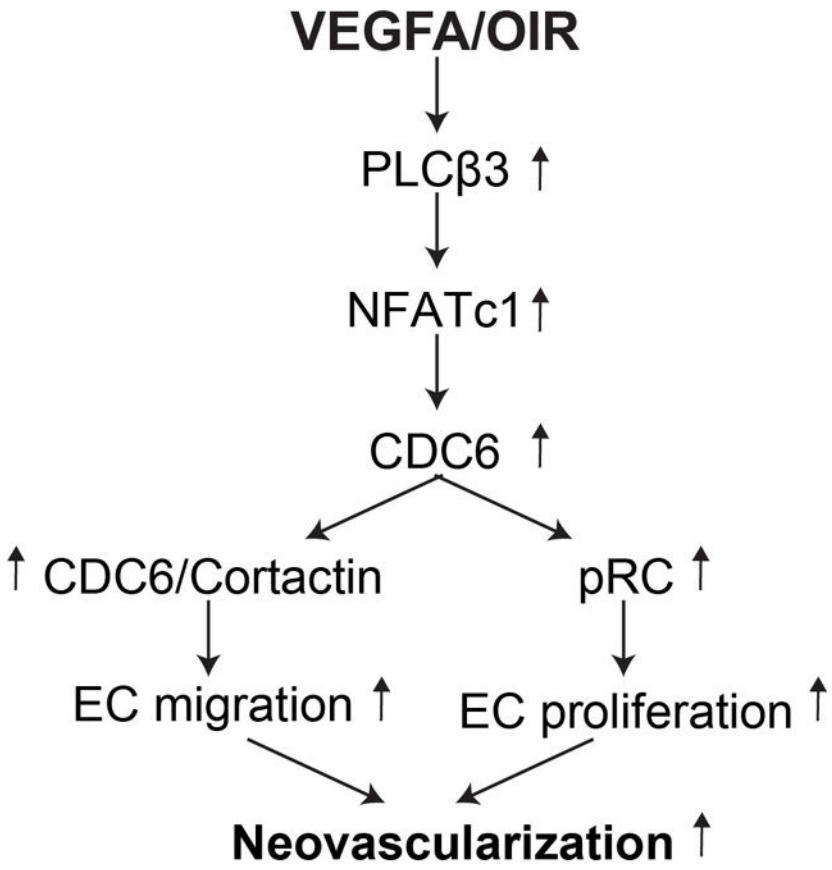

Keywords

cell division cycle 6; nuclear factor of activated T cells c1; oxygen-induced retinopathy; phospholipase Cβ3; retinal neovascularization; vascular endothelial growth factor A

INTRODUCTION

The eye are perhaps the most important organ of our five senses, and they play a critical role in visual sensations that capture some of the best features of life. Visual impairment or blindness can result in a struggle to perform even the most routine work across an individual's lifespan. Globally, 146 million adults suffer from impaired vision due to diabetic retinopathy (DR), accounting for a global prevalence of 34.6% of all diabetic individuals (1). However, according to the most recent World Health Organization's (WHO) World Report on Vision, out of 2.2 billion people globally with vision impairment in 2019, the vision loss in at least 1 billion individuals could have been prevented (2). Depending on the extent of vascular lesions and severity, DR is categorized into mild, moderate, nonproliferative, and proliferative states, among which proliferative DR (PDR) is characterized by abnormal capillary growth, neovascularization, microaneurysm and dilation, hemorrhage, and plasma leakage (3). In contrast to neovascularization in the skin during wound repair, retinal neovascularization is not productive and instead deteriorates the underlying tissue condition (4,5). Neovascularization occurs in the retina

due to disruption of oxygen and nutrient supply, and it drives dysregulated expression of angiogenic growth factors promoting abnormal angiogenesis (6–8). Further, the dysregulated angiogenesis affects the metabolic demand, impairing retinal function (6, 8–9). Thus, retinal neovascularization is the most common cause of vision loss among all ocular diseases including retinopathy of prematurity (ROP), DR, and age-related macular degeneration (AMD) (10–12). During the last several decades, the development of animal models that mimic these vascular eye diseases significantly advanced our understanding of the crucial role of vascular endothelial growth factor (VEGF) in retinal neovascularization. This led to the development of anti-VEGF therapies (13,14). However, current anti-VEGF therapies for retinal neovascularization have limitations. First, anti-VEGF drugs effectively treat neovascularization only in some, but not all, patients (15,16). Second, long-term use of anti-VEGF drugs cause degeneration of normal blood vessels, apoptosis, and angiofibrosis of neural retina and choroid, ultimately resulting into vitreous hemorrhage (17–21). Therefore, specific and better therapeutic targets are needed for the effective treatment of vision-threatening ocular neovascularization.

VEGFA elicits most of its cellular effects via activation of its receptor VEGFR2 both in physiological and pathological conditions (22–24). VEGFA, through its interaction with VEGFR2, triggers activation of phospholipases such as PLCγ1, releasing intracellular calcium (25). Many studies have shown that increased intracellular calcium via stimulation of calcineurin leads to dephosphorylation and activation of nuclear factors of activated T cells (NFATs) in the regulation of immune cell responses and the migration and proliferation of various other cell types (26). Among the five members of the NFAT family, NFATc3 was reported to regulate COX2 expression in endothelial cells, promoting their migration and angiogenesis (27). Furthermore, it was reported that cyclosporin A (CsA), a pharmacological inhibitor of calcineurin and thereby NFATs, blocks angiogenic effects of VEGF in mouse retinal microvascular endothelial cells (28). In addition, Suehiro et al., (29) reported that NFATc1, via its dynamic binding to the promoters of angiogenesis-related genes and their regulation, plays a critical role in VEGF-mediated endothelial cell barrier function, migration, and tube formation. Cell division cycle 6 (CDC6) is an important factor in regulating minichromosomal maintenance (MCM)-chromatin interactions to form pre-replication complexes in the DNA and promote cell cycle progression through the G1/S checkpoint (30). Apart from its essential role in DNA replication, some reports also showed that CDC6 plays a role in cell migration (31–33). Since both CDC6 and NFATs play a role in cell proliferation and migration, and endothelial cell migration and proliferation are essential for angiogenesis, we questioned whether NFATc1 has any link to CDC6 regulation and, if so, does the NFATc1-CDC6 axis have any influence on retinal neovascularization? To this end, our results for the first time show that PLCβ3-NFATc1 axis-mediated CDC6 expression plays a crucial role in VEGFA/VEGFR2-induced angiogenic events of human retinal microvascular endothelial cells and retinal neovascularization in oxygen-induced retinopathy (OIR) mouse model.

MATERIALS AND METHODS

The data that support the findings of this study are available from the corresponding author on reasonable request.

Reagents:

Recombinant human VEGF165a (Cat. No. 293-VE-010/CF) and recombinant mouse VEGF164a (Cat. No. 493-MV- 025/CF) were bought from R&D Systems (Minneapolis, MN). Growth factor- reduced Matrigel (Cat. No. 354230) was purchased from BD Biosciences (Bedford, MA). Anti-CDC6 (sc-9964), anti-Cortactin (sc-55579), anti-MCM2 (sc-9839), anti-MCM3 (sc-9850), anti-MCM4 (sc-28317), anti-MCM5 (sc-165995), anti-MCM6 (sc-9843), anti-MCM7 (sc-9966), anti-MEK1 (sc-6250), anti-p53 (sc-126), anti-PLCβ1 (sc-5291), anti-PLCβ2 (sc-9018), anti-PLCβ3 (sc-13323), anti-PLCβ4 (sc-166131), and anti-β-Tubulin (sc-5274) antibodies were obtained from Santa Cruz Biotechnology (Santa Cruz, CA). Mouse anti-CD31 antibody (Cat. No. 550274) was bought from BD Pharmingen (Palo Alto, CA). Anti-Ki67 (ab15580), and anti-pSer/Thr (ab17464) antibodies, Fluo-8 calcium flux assay kit (ab112129) and Fluo-8 AM green fluorescent calcium binding dye (ab142773) were obtained from Abcam (Cambridge, MA). Anti-HIF1α (Cat. No. 14179), anti-PLCγ1 (Cat. No. 2822), anti-pPLCγ1 (Y783) (Cat. No. 2821), and anti-VEGFR2 (Cat. No. 2479) antibodies were obtained from Cell Signaling Technology (Danvers, MA). Mouse anti-CD31 antibody (Cat. No. 550274) was bought from BD Pharmingen (Palo Alto, CA). Anti-pTyr antibody (PY20) (Cat. No. 05–777) was obtained from EMD Millipore (Burlington, MA). ViaStain ™ AOPI staining solution (CS2–0106) and SD100 slides (CHT4-SD100–014) were from Nexcelom Bioscience (Lawrence, MA). Human CDC6 siRNA (Id: s2744), human NFATc1 siRNA (Id: s9470), human PLCβ1 siRNA (Id: 136825), human PLCβ3 siRNA (Id: s10619), and human PLCg1 siRNA (Id: s10632) were bought from Thermo Scientific (Chicago, IL). Control non-targeting siRNA (D-001810–10), mouse CDC6 siRNA (L-043543–00-0020), mouse NFATc1 siRNA (L-054700–00-0020), and mouse PLCβ3 siRNA (L-040969–01-0020) were obtained from Dharmacon (Pittsburgh, PA). [^{3}H]-Thymidine (S.A. 20 Ci/mmole) was bought from Perkin Elmer (Boston, MA). Endothelial basal medium (EBM) (CC-3133), and endothelial growth medium (EGM) SingleQuot kit supplements and growth factors (CC-4133) were purchased from Lonza (Walkersville, MD). Cytodex microcarrier beads (Cat. No. C3278), thrombin (Cat. No. T8885), and anti-vinculin antibody (Cat. No. V9131) were obtained from Sigma Aldrich (St Louis, MO). Fibrinogen (Cat. No. 820224) was procured from MP Biomedicals LCC (Solon, OH). Anti-NFATc1 antibody (Cat. No. MA3–024), Dyna beads (Cat. No. 11035), Invivofectamine 3.0 (Cat. No. IVF3001), Phalloidin (Cat. No. A12380), and lipofectamine 3000 transfection reagent (Cat. No. L-3000–015) were purchased from Thermo Fisher Scientific (Waltham, MA). Isolectin B4–594 (I21413), cell tracker green (C7025), goat anti-rabbit IgG-AlexaFluor 488 (A11034), goat anti-rat IgG-AlexaFluor 568 (A11077), goat anti-rat IgG-AlexaFluor 350 (A21093), Hoechst 3342, and Prolong Gold antifade reagent (P36930) were bought from Molecular Probes (Eugene, OR).

Retroviral vectors:

The CDC6 overexpression retroviral CLXSN 5myc-CDC6-WT plasmid was a gift from Jean Cook (Addgene plasmid #109332; http://n2t.net/addgene:109332; RRID:Addgene_109332) (34). Empty retroviral pCLXSN (Addgene plasmid #12343; http://n2t.net/addgene:12343; RRID:Addgene_12343) and pCL-Eco (Addgene plasmid #12371; http://n2t.net/addgene:12371; RRID:Addgene_12371) plasmids were gifts from Inder Verma (35). pMD2.G plasmid (Addgene plasmid #12259;http://n2t.net/addgene:12259;

RRID:Addgene_12259) was a gift from Didier Trono. To produce retroviral particles, HEK 293A cells were co-transfected with CLXSN 5myc-CDC6-WT or pCLXSN plasmid along with pMD2.G (envelope) and pCL-Eco (gag/pol/env) according to Addgene Lentivirus Production protocol and, after the appearance of cytopathy, the virus was collected, amplified, and purified by cesium chloride gradient centrifugation. The titer was determined by plaque assay as described previously (36). The retroviral particles were used at a final concentration of 40 moi.

Plasmids:

Human cortactin Y421F, Y446F, Y453F, Y470F, and Y486F plasmids were constructed as described previously (37).

Animals:

C57BL/6J (WT) pregnant mice (strain code 027) at E16 were obtained from Charles River Laboratories (Wilmington, MA). PLCβ3$^{-/-}$ mice (stock # 019023) were purchased from The Jackson Laboratory (Bar Harbor, ME). NFATc1$^{flox/flox}$ mice were obtained from Dr. Laurie H. Glimcher at Harvard Medical School (Boston, MA). Cdh5-Cre^{ERT2} mice were obtained from Dr. Luisa Iruela-Arispe at the University of California in Los Angeles, CA. To delete NFATc1 in endothelium during postnatal development, we interbred NFATc1$^{flox/flox}$ mice with Cdh5-Cre^{ERT2} mice to generate NFATc1$^{flox/-}$:Cdh5-Cre^{ERT2} mice. These mice were then backcrossed with NFATc1$^{flox/flox}$ mice to generate NFATc1$^{flox/flox}$:Cdh5-Cre^{ERT2} litters. To induce Cre activity, two consecutive intraperitoneal injections of tamoxifen (50 μl) (Sigma Aldrich, T5648; 2 mg/ml in 10% ethanol and 90% corn oil) were given to mice pups at P9 and P10 to delete NFATc1 in the endothelium (NFATc1$^{i\Delta EC}$). Tamoxifen was also injected into WT mice pups as a control. Mice were bred and maintained at the University of Tennessee Health Science Center's vivarium. All experiments involving animals were approved by the Institutional Animal Care and Use Committee (IACUC) of the University of Tennessee Health Science Center (Memphis, TN).

Isolation of mouse retinal microvascular endothelial cells (MRMVECs) and aortic smooth muscle cells (MASMCs):

Sheep anti-rat Dyna beads were washed three times with serum-free DMEM and then incubated with rat anti-mouse CD31 antibody overnight at 4°C (10 μl antibody/50 μl beads in DMEM). Eyes from 3-wk old WT or NFATc1$^{i\Delta EC}$ mice pups were enucleated, and retinas were dissected out and kept in PBS containing penicillin/streptomycin. Retinas were then washed with PBS, minced into small pieces using sterilized razor blade, and then digested in 4 ml of collagenase type I (1 mg/ml in serum-free DMEM) (Cat. No. LS004196, Worthington, Lakewood, NJ) for 60 min at 37°C. Following digestion, DMEM with 10% fetal bovine serum (FBS) was added, the mixture was filtered through a sterile 40-μm nylon mesh (Cat. No. 352340, BD Biosciences, San Jose, CA), and then centrifuged at 1000 rpm for 5 min to pellet the cells. After washing with DMEM containing 10% FBS twice, the cell pellet was resuspended in 1 ml DMEM with 10% FBS and incubated with sheep anti-rat magnetic beads coated with anti-CD31 antibody overnight. The beads were washed six times with DMEM containing 10% FBS and the bound cells were plated onto a single well of a 24-well plate. Endothelial cells were grown in EGM-2 medium containing 20% FBS. Cells

were maintained at 37°C with 5% CO_2 atmosphere and propagated in 1% gelatin-coated dishes. MASMCs were isolated and grown as described by us previously (38).

Cell culture:

HRMVECs (Cat. No. ACBRI 181) were purchased from Cell Systems (Kirkland, WA) and grown in EGM containing growth supplements, 10 μg/ml gentamycin, and 0.25 μg/ml amphotericin B. Human fibroblasts (Cat. No. PCS-201–013) were obtained from American Type Culture Collection (Manassas, VA) and grown in EGM containing growth supplements, 10 μg/ml gentamycin, and 0.25 μg/ ml amphotericin B. Cultures were maintained at 37°C in a humidified 95% air and 5% CO_2 atmosphere. HRMVECs with passage numbers between 5 and 10 were synchronized by maintaining in growth factor-free EBM for 24 hrs and were used to perform experiments unless otherwise indicated.

Cell viability:

HRMVEC viability after transfection with non-targeted or targeted siRNA and quiescence in serum-free EBM2 was measured as follows. To 20 μl of cell suspension, 20 μl of AOPI staining solution was added in a micro centrifuge tube and mixed by pipetting up and down for 3 times. Then 20 μl of the mixure was loaded onto a counting chamber (SD100 slide). The AO/PI-positive cells were examined under a automated fluorescent viability cell counter (Cellometer Auto 2000) and the % live cells was determined by calculating PI-positive cells/AO-positive cells x 100.

Calcium release assay:

HRMVECs transfected with non-targeted or targeted siRNA were seeded onto a 96-well plate (50,000 cells/well), quiesced for 24 hrs in serum-free EBM2 and washed with HBSS. The cells were then pre-loaded with Fluo-8 AM fluorescent dye according to manufacturer's instructions. In brief, 1X assay buffer was prepared by mixing 9 ml of HHBS with 1 ml of 10X Pluronic F127 Plus solution. Then, 20 μl of Fluo-8 stock solution was added to 10 ml of 1X assay solution to make 5 μM Fluo-8 dye loading solution. One hundred microliters of Fluo-8 dye loading solution was added to each well containg cells and incubated at 37°C for 30 min followed by standing at room temperature for 30 min. After incubation, cells were washed 2 times with HBSS and treated with vehicle or VEGFA (40 ng/ml) for the indicated time periods, at which time the fluorescence readings were measured in a SpectraMax Gemini XPS fluorescence micro plate reader at 490 nm excitation and 525 nm emission. The iCalcium release was expressed as fold change over control.

Calcium staining:

HRMVECs transfected with non-targeted or targeted siRNA were seeded onto a coverslip, quiesced for 24 hrs in serum-free EBM2 and washed with HBSS. The cells were then pre-loaded with Fluo-8 AM using manufacturer's instructions. Fluo-8 green dye (5 μM) prepared in HBSS was added, and cells were then incubated at 37°C for 30 min followed by standing at room temperature for 30 min. Cells were washed 2 times with HBSS and treated with vehicle or VEGFA (40 ng/ml) for 30 min. After the treatments, the coverslips containing cells were washed with HBSS for 2 times, fixed with 4% paraformaldehyde,

mounted on a slide with ProLong Gold anti-fade mounting medium, observed under Zeiss inverted microscope (Axiovision Observer.z1; 40X/NA 0.6) and the fluorescence images were captured using Zeiss AxioCam MRm camera and the microscope operating and image analysis software AxioVision 4.7.2 (Carl Zeiss Imaging Solutions GmbH).

Cell migration:

HRMVEC and MRMVEC migration was measured by wound-healing assay essentially as described previously (38). Briefly, HRMVECs or MRMVECs were plated at 2 X 10^5 cells/ml in each chamber of the ibidi culture inserts and grown to full confluency. Following a 24 hrs growth arrest period in EBM, the inserts were removed using sterile tweezers and 1 ml of EBM containing 5 mM hydroxyurea was added. Cells were treated with and without VEGFA (40 ng/ml) for 24 hrs at which time period the migrated cells were observed under a Nikon Eclipse TS100 microscope with a 4X/0.13 NA objective, and the images were captured with a Nikon Digital Sight DS-L1 camera. Cell migration was expressed as percentage of wound closure (total area minus area not occupied by the cells/total area X 100). Wherever siRNA or plasmids or retroviral vectors were used, cells were transfected with either non-targeted or on targeted siRNA or pCMV empty vector or expression vector for the indicated gene or infected with empty or CDC6 overexpressing retrovirus and then allowed to grow to 70–80% confluence. Cells were then trypsinized, plated at 2 X 10^5 cells/ml in each chamber of the ibidi culture inserts and subjected to migration assay.

PLCβ activity:

PLCβ activity was measured as described previously (36). PLCglow (WH-15) fluorescent substrate (KXTbio, Chapel Hill, NC) was used to measure PLC activity. In brief, HRMVECs were treated with and without VEGFA (40 ng/ml) for the indicated time periods, and cell extracts containing equal amounts of protein from control and each treatment were immunoprecipitated with anti-PLCβ1 or anti-PLCβ3 antibodies. The immunocomplexes were suspended in 50 μl of reaction buffer (50 mM 4-(2-hydroxyethyl)-1-piperazineethanesulfonic acid, pH 7.2, 250 mM KCl, 1 mM CaCl2, 2 mM dithiothreitol [DTT], 50 μg/ml BSA, and 0.5% sodium cholate) containing 10 μM PLCglow and incubated for 90 min at room temperature with gentle rocking. The reaction was quenched with the addition of five volumes of 10 mM ethylene glycol tetraacetic acid. After centrifugation at 2000 rpm for 5 min, the supernatant was transferred to a 96-well plate and the fluorescence intensity was measured using a SpectraMax Gemini XS spectrofluorometer (Molecular Devices, Sunnyvale, CA) at 344-nm excitation and 530-nm emission. PLCβ activity was expressed as fold changes in fluorescence intensity as compared to control. Fluorescence intensity was proportional to enzyme activity (39).

DNA synthesis:

DNA synthesis was measured by [^{3}H]-thymidine incorporation as described previously (40). Briefly, cells were transfected with either targeted or non-targeted siRNA or pCMV or CTTN (Y470F) plasmids or were infected with empty or CDC6 overexpressing retrovirus. Cells were then plated onto 6-well plates, allowed to grow to 70–80% confluence, synchronized for 24 hrs, and then treated with or without VEGFA (40 ng/ml) for 24 hrs. After 6 hrs of VEGFA addition, cells were pulse-labeled with 1 μCi/ml of [^{3}H]-thymidine

for 18 hrs. After a 24 hrs incubation period, cells were washed with cold PBS, trypsinized, and pelleted by centrifugation. The cell pellet was resuspended in 3 ml of 20% (w/v) cold TCA and vortexed vigorously to lyse cells. The mixture was kept on ice for 30 min and then passed through a GF/F glass microfiber filter. The filter was washed first with 3 ml of 5% cold TCA and then 3 ml of cold ethanol, dried, placed in a liquid scintillation vial containing 5 ml of scintillation fluid and the radioactivity was counted in a liquid scintillation counter (Beckman LS 3801). DNA synthesis was expressed as fold changes in cpm per dish over control.

Three-dimensional (3D) sprouting assay:

Three-dimensional sprouting assay was performed as described previously (40). Briefly, cells were transfected with either targeted or non-targeted siRNA or pCMV or CTTN (Y470F) plasmids, or were infected with empty or CDC6 overexpressing retrovirus. Cells were labeled with a cell tracker, trypsinized, pelleted, and an equal number of cells were coated onto Cytodex beads for 6 hrs. Non-binding cells were then washed with PBS and the beads were embedded in fibrin gel. Human fibroblasts suspended in EGM with and without VEGFA (40 ng/ml) were seeded onto the top of the fibrin gel at a concentration of 2×10^4 cells/well and incubated at 37°C for 6 hrs, at which time the medium was replaced with fresh EGM with and without VEGFA, and incubation continued for three days. Sprouting was examined on day 3 under a Zeiss inverted fluorescence microscope (AxioVision Observer.z1; 10X/NA 0.45) and the fluorescence images were captured using a Zeiss AxioCam MRm camera and the microscope operating and image analysis software Zen 2.6 (blue edition) (Carl Zeiss Imaging Solutions GmbH). Sprouting was expressed as number of sprouts per bead.

Tube formation:

Tube formation was measured as described previously (40). Briefly, cells were transfected with either targeted or non-targeted siRNA or pCMV or CTTN (Y470F) plasmids, or were infected with empty or CDC6 overexpressing retrovirus. Cells were synchronized for 24 hrs and plated in a 24-well culture plate coated with growth factor-reduced Matrigel. Cells were added with or without VEGFA (40 ng/ml) and incubation continued for 6 hrs at 37°C. Tube formation was observed under an inverted phase contrast microscope (Eclipse TS100; Nikon, Tokyo, Japan) and the images were captured with CCD color camera (KP-D20AU; Hitachi, Ibaraki, Japan) using Apple iMovie 7.1.4 software. Tube length was calculated using NIH ImageJ version 1.53 software and expressed in micrometers.

Podosome formation:

Podosome formation was measured as described by Biosse et al. (41). Cells were transfected with either targeted or non-targeted siRNA or pCMV or CTTN (Y470F) plasmids, plated over cover slips placed into 6-well plates, allowed to grow to 70–80% confluence, synchronized for 24 hrs, and then treated with or without VEGFA (40 ng/ml) for 2 hrs. After the incubation period, cells were washed with cold PBS, fixed in 4% paraformaldehyde, permeabilized with 0.3% Triton X100, and blocked with 3% BSA. The cells were then incubated with anti-Vinculin antibody (1:100) overnight followed by incubation with Alexa Fluor 488-conjugated goat anti-mouse secondary antibody in combination with Alexa

Fluor™ 568 Phalloidin. The cells were then observed under a Zeiss inverted microscope (Axiovision Observer.z1; 40X/NA 0.6 or 10X/NA 0.45) and the fluorescence images were captured by a Zeiss AxioCam MRm camera using the microscope operating and image analysis software Zen 2.6 (blue edition) (Carl Zeiss Imaging Solutions GmbH). Podosomes were identified by visualizing F-actin/Vinculin coimmunolocalization at the edge of each cell. Podosome formation was expressed as number of podosomes/cell.

Western blotting:

After appropriate treatments, cell or retinal extracts were prepared and an equal amount of protein from control and each treatment was resolved by electrophoresis on SDS-polyacrylamide gels. The proteins were transferred electrophoretically onto a nitrocellulose membrane. After blocking in 5% (w/v) non-fat dry milk or BSA for 1 hr, the membrane was incubated with the indicated primary antibody overnight at 4°C. The membrane was then washed with TBST 3 times, 10 min each, and then incubated with horseradish peroxidase-conjugated secondary antibody for 1 hr. After washing again with TBST 3 times, 10 min each, the membrane was then incubated with enhanced chemiluminescence reagents (Amersham Biosciences) and the antigen-antibody complexes were detected by exposure to x-ray film and developed in an x-ray film developer.

Transfections and infections:

HRMVECs or MRMVECs were transfected with either targeted or non-targeted siRNA (100 nmoles) or plasmid DNA (1 μg/ml) using Lipofectamine 3000 transfection reagent according to the manufacturer's instructions. After 6 hrs of incubation, cells were recovered in EGM for 30 hrs, synchronized overnight in EBM, and used as needed. HRMVECs were infected with empty or CDC6 overexpressing retrovirus at final concentration of 40 moi and, after 12 hrs of infection, cells were recovered in EGM for 24 hrs, synchronized overnight in EBM, and used as needed.

Oxygen-induced retinopathy (OIR):

OIR was performed as per the method of Smith et al., (42) and quantified as per the protocol of Connor et al., (43) and as described by us previously (44). C57BL/6J, NFATc1$^{flox/flox}$:Cdh5-Cre^{ERT2} and PLCβ3$^{-/-}$ mice pups at P7 along with their dams were exposed to 75% oxygen for 5 days and then returned to room air at P12 to develop hyperoxia-mediated hypoxia (post-OIR). Mice pups of the same age kept at room air were used as controls. All the pups were sacrificed at P17 and eyes were enucleated and fixed in 4% (w/v) paraformaldehyde for 1 hr at room temperature. Retinas were isolated and stained with isolectin B4, flat mounts were made, placed under a coverslip and examined under a Zeiss inverted fluorescence microscope (Axiovision Observer.z1). Retinal neovascularization was quantified by first setting a scale with a tolerance point of 50 based on the fluorescence intensity in the screenshot using Nikon NIS-Elements software version AR31. Neovascularity was highlighted in red (false color) and then quantified by dividing the fluorescence intensity in the highlighted area by the total fluorescence intensity in the screenshot. Small interference RNA (siRNA) solutions were prepared by mixing equal volume of siRNA duplex (at 4 mg/ ml) with an equal volume of complexation buffer, which was then mixed with an equal volume of invivofectamine 2 transfection reagent (Thermo

Fisher). The invivofectamine 2-siRNA duplex mixtures were then incubated at 50°C for 30 min followed by dilution (6X) with PBS. The resulting mixture was concentrated using Amicon Ultra-15 Ultracel-50K filters to achieve the final concentration of siRNA to 2.0 mg/ml. Non-targeted or on-targeted siRNA at 1 μg/0.5 μl/eye was injected into mice pups at the indicated time periods of hyperoxia or relative hypoxia by intravitreal injections using a 33G needle. Empty reterovirus (EVir) or CDC6 overexpressing reterovirus (CDC6 Vir) suspended in sterile PBS were injected intravitreally at 40 moi/0.5 μl/eye.

Immunofluorescence staining:

At the end of 5 days of hyperoxia period (P7-P12), mice pups were returned to room air. After 72 hrs of room air (P15), pups were sacrificed, eyes were enucleated, fixed in optimal cutting temperature compound, and 8-μm cryosections were made from the central part of the retina. After blocking in normal goat serum, the cryosections were probed with either anti-Ki67 antibody (1:100) or anti-CDC6 antibody (1:50) or anti-NFATc1 antibody (1:100) in combination with rat anti-CD31 antibody (1:100) followed by incubation with Alexa Fluor 568-conjugated goat anti-rabbit/mouse and Alexa Fluor 488-conjugated goat anti-rat secondary antibodies. The sections were then observed under a Zeiss inverted microscope (Axiovision Observer.z1; 40X/NA 0.6 or 10X/ NA 0.45) and the fluorescence images were captured by a Zeiss AxioCam MRm camera using the microscope operating and image analysis software Zen 2.6 (blue edition) (Carl Zeiss Imaging Solutions GmbH).

Statistics:

Since mice pups from P6 to P17 were used in the experiments, and pups are sexually immature, sex differences were not expected to influence the observations. Therfore, we did not perform the experiments sex wisely. All experiments were repeated three times and the data are presented as Mean ± SD. Normality of the data (using D'Agostino-Pearson normality test) and the equality of group variance (using F test) were performed on all data using GraphPad Prism v 8.00 software. The normally distributed data with similar variance were analyzed by one-way ANOVA followed by Fisher's least significant difference post hoc test or two-tailed student "t" test and the p values <0.05 were considered statistically significant. Samples sizes were estimated based on previous studies (40,44).

RESULTS

CDC6 mediates VEGFA-induced HRMVEC proliferation, migration, podosome formation, sprouting, and tube formation in vitro and OIR-induced retinal neovascularization in vivo

VEGFA plays a major role in physiological and pathological angiogenesis by stimulating endothelial cell (EC) functions such as proliferation, migration, and differentiation that are required for new blood vessel formation (5,8). CDC6 plays an indispensable role in pre-replication complex (pRC) formation and thus in DNA replication (30). Besides its well-established role in cell cycle progression, some studies have reported that CDC6 also plays a role in cell migration (31–33). Furthermore, we reported that CDC6 plays a role in VSMC proliferation and neointima formation (45). Thus, all these observations point out a role for CDC6 in both cell proliferation and migration. As EC migration and proliferation are two impotant events of angiogenesis and in view of the involvement of CDC6 in the

modulation of both cell proliferation and migration, we questioned whether CDC6 plays a role in retinal neovascularization. VEGFA but not VEGFB or VEGFC induced CDC6 expression in a time-dependent manner in human retinal microvascular endothelial cells (HRMVECs) (Figure 1A). As CDC6 first assembles with origin replication complex and then loads minichromosome maintenance protein complex (MCM) to form a pRC, we tested the time course effect of VEGFA on MCM levels. No apparent changes were observed in the levels of MCM proteins (namely MCM2, MCM3, MCM4, MCM5, MCM6 and MCM7) between control and VEGFA-treatments (Figure 1A). Based on these observations, we next tested the role of CDC6 in VEGFA-induced angiogenic responses of HRMVECs. Small interference RNA (siRNA)-mediated downregulation of CDC6 levels inhibited VEGFA-induced HRMVEC proliferation, migration, sprouting, and tube formation (Figure 1B–E). In order to rule out that the observed decreases in HRMVEC proliferation, migration, sprouting and tube formation by CDC6 depletion were not due to cell death, we studied the effect of CDC6 depletion by its siRNA on HRMVEC viability. Depletion of CDC6 by its siRNA had no effect on HRMVEC survial (Figure 1F). It was demonstrated that podosomes play an important role in cell crawling and migration (46). Therefore, we tested CDC6's role in podosome formation. Depletion of CDC6 levels by its siRNA substantially inhibited VEGFA-induced podosome formation (Figure 1G). Podosomes consist of an F-actin-rich core that is comprised of a subset of actin-regulatory proteins including cortactin (47). In addition, many studies have shown that phosphorylation of cortactin at tyrosine residues enhances actin assembly and podosome formation (48). Therefore, we asked whether CDC6-mediated podosome formation requires the involvement of cortactin. First, VEGFA induced tyrosine phosphorylation of cortactin in a time-dependent manner in HRMVECs (Figure 1H). Second, out of five potential tyrosine phosphorylation sites identified in human cortactin (37), VEGFA-induced phosphorylation occurred at Y421, Y453, and Y470 but not at Y446 and Y486 residues (Figure 1I). Third, VEGFA induced a complex formation between CDC6 and cortactin in a time-dependent manner in HRMVECs (Figure 1J). Fourth, phosphorylation of cortactin at Y470 but not Y421 or Y453 is required for its interaction with CDC6 (Figure 1K). In view of these findings, we then tested the role of cortactin phosphorylation in VEGFA-induced podosome formation. To this end, overexpression of cortactin Y470F mutant inhibited VEGFA-induced podosome formation both in HRMVECs and MRMVECs (Figure S1D & H). In line with these observations, overexpression of cortactin Y470F mutant also blocked VEGFA-induced migration, sprouting, and tube formation of both HRMVECs and MRMVECs (Figure S1A–C & E–G). Based on the role of CDC6 in EC proliferation, podosome formation, migration, sprouting, and tube formation, we next examined its role in retinal neovascularization. OIR-mediated hypoxia induced CDC6 expression in a time-dependent manner in the mouse retina (Figure 2A, upper panel). To confirm that CDC6 was induced by post-OIR, its levels were measured at P6, P10 and P13 of normoxia, at 72 hrs of hyperoxia (i.e., pups exposed to hyperoxia from P7 to P10) and at 24 hrs of post-OIR (i.e., pups after exposure to hyperoxia from P7 to P12 returned to room air for 24 hrs, P13). As one can see CDC6 was expressed in P6 retina and it was reduced in a time dependent manner up until P13, disaapered completely at 72 hrs of hyperoxia, and then induced abundantly at 24 hrs of hyperoxia-mediated hypoxia, i.e., 24 hrs post-OIR (Figure 2A, bottom panel). To validate the hyperoxia-mediated hypoxia in the retina, the retinal extracts were also analyzed for HIF1α levels. It was indeed exciting

to observe that HIF1α that was present at basal levels in P6, P10 and P13 retinas of normoxia, completely disappeared at 72 hrs of hyeroxia and induced by manyfold at 24 hrs of post-OIR (Figure 2A, bottom panel). These findings clearly suggest the responsiveness of CDC6 induction by hypoxia. Furthermore, coimmunostaining for CDC6 and CD31 showed that OIR induces CDC6 expression predominantly in retinal ECs (Figure 2B). In addition, downregulation of CDC6 levels by its siRNA reduced OIR-induced retinal neovascularization with decreased EC proliferation, density of tufts, and filopodia formation (Figure 2C–F). It is interesting to note that the avascular area was found to be decreased in CDC6-depleted retinas as compared to retinas treated with non-targeted siRNA in response to OIR (Figure 2C & D). Together, these results clearly indicate that OIR-induced CDC6 expression is required for retinal neovascularization.

NFATc1 mediates VEGFA-induced CDC6 expression, HRMVEC proliferation, migration, sprouting, and tube formation in vitro and OIR-induced retinal neovascularization in vivo

Previously, we reported that NFATc1 mediates thrombin-induced CDC6 expression in human aortic smooth muscle cells (45). Thus, to understand the upstream mechanisms by which VEGFA induces CDC6 expression, we tested the role of NFATc1. Depletion of NFATc1 levels by its siRNA completely inhibited VEGFA-induced CDC6 expression in HRMVECs (Figure 3A). This result indicates that VEGFA-induced CDC6 expression is dependent on NFATc1 activation. Based on this finding, we next tested the role of NFATc1 in VEGFA-induced HRMVEC proliferation, migration sprouting, and tube formation. Depletion of NFATc1 levels also blocked VEGFA-induced HRMVEC proliferation, migration, sprouting, and tube formation (Figure 3B–E). Together, these observations reveal that upstream to CDC6 expression, activation of NFATc1 is required for VEGFA-induced angiogenic events of HRMVECs. Based on these observations, we next examined the role of NFATc1 in retinal neovascularization using two approaches. In the first approach, we used siRNA to deplete NFATc1 levels in the mouse pups' retinas and studied its role in OIR-induced CDC6 expression and retinal neovascularization. As expected, depleting NFATc1 levels by its siRNA suppressed OIR-induced CDC6 expression in the mouse pups' retinas (Figure S2A). Furthermore, NFATc1 depletion also attenuated OIR-induced retinal neovascularization, retinal EC proliferation, density of tufts and filopodia formation with increased avascular area (Figure S2B–E). In another approach, we used EC-specific NFATc1 knockout mice. Basically, NFATc1$^{fl/fl}$:Cdh5Cre^{ERT2} transgenic mice pups received tamoxifen injections to induce Cre activity and thereby delete NFATc1 in ECs (NFATc1$^{i\Delta EC}$), and we used these pups for OIR-induced retinal neovascularization. Tamoxifen was also injected into WT mice as a control. Tamoxifen injections resulted in the depletion of NFATc1 only in ECs but not in SMCs (Figure 4A, upper panel). In addition, coimmunostaining for CD31 and NFATc1 showed that NFATc1 levels were completely depleted in both normoxic and post-OIR retinas of NFATc1$^{i\Delta EC}$ mice pups as compared to retinas of WT mice pups (Figure 4A, bottom panel). We next tested the role of EC-specific NFATc1 deletion in hypoxia-induced CDC6 expression. As expected, OIR induced CDC6 expression as compared to normoxia in the retinas (mostly in ECs) of WT mice pups (Figure 4B). However, OIR had little or no effect on CDC6 expression in the retinal ECs of NFATc1$^{i\Delta EC}$ mice pups (Figure 4B). In addition, the tendency of CDC6 expression was found to be more in the angiogenic front towards the optic nerve in the case of OIR model

and towards periphery during development (Figure 4B & C). These observations imply that OIR-induced CDC6 expression occurs in retinal ECs and that this effect was dependent on NFATc1 activation. Consistent with these observations, EC-specific deletion of NFATc1 also reduced retinal neovascularization, retinal EC proliferation, and attenuated tufts and filopodia formation resulting in increased avascular area as compared to WT mice pups (Figure 4D–G). Together, these results affirm that OIR-induced CDC6 expression and retinal neovascularization were dependent on activation of NFATc1.

Expression of CDC6 rescues VEGFA-induced MRMVEC proliferation, migration, podosome formation, sprouting and tube formation from inhibition by EC-specific NFATc1 deletion in vitro and OIR-induced retinal neovascularization in vivo

In order to obtain additional evidence on the role of the NFATc1-CDC6 axis in regulating retinal neovascularization, we isolated retinal ECs from WT and NFATc1$^{i\Delta EC}$ mice and tested the effects of VEGFA on CDC6 expression, proliferation, podosome formation, migration, sprouting and tube formation. As expected, VEGFA induced CDC6 expression in retinal ECs of WT mice but not NFATc1$^{i\Delta EC}$ mice (Figure S3A). In line with these observations, retinal ECs from NFATc1$^{i\Delta EC}$ mice were resistant to VEGFA-induced proliferation, podosome formation, migration, sprouting, and tube formation as compared to retinal ECs from WT mice (Figure S3B–F). Next, we performed the rescue experiments using CDC6 overexpressing retroviral particles in retinal ECs of NFATc1$^{i\Delta EC}$ mice. We found that retroviral-mediated CDC6 expression rescues VEGFA-induced EC proliferation, migration, sprouting, and tube formation from inhibition by lack of NFATc1 in the retinal ECs of NFATc1$^{i\Delta EC}$ mice (Figure 5A–D). Based on these in vitro findings, we next performed the rescue experiments in vivo. To this end, we injected CDC6 overexpressing retrovirus intravitreally into NFATc1$^{i\Delta EC}$ mice and tested the effect of OIR on retinal neovascularization. As expected, OIR induced retinal neovascularization, retinal EC proliferation, density of tufts and filopodia formation in WT mice and these effects were blunted in NFATc1$^{i\Delta EC}$ mice. However, retroviral-mediated overexpression of CDC6 rescued OIR-induced retinal neovascularization, retinal EC proliferation, density of tufts, and filopodia formation with decreased avascular area as compared to NFATc1$^{i\Delta EC}$ mice injected with empty retrovirus (Figure 6A–D). Together, these observations further confirm the role of the NFATc1-CDC6 axis in VEGFA-induced EC angiogenic responses and OIR-induced retinal neovascularization.

PLCβ3 acts upstream to NFATc1 in inducing CDC6 expression and in modulating activation of VEGFA-induced HRMVEC proliferation, migration, sprouting, and tube formation in vitro and OIR-induced retinal neovascularization in vivo

Ca^{2+}/calmodulin-mediated activation of protein phosphatase calcineurin is required for dephosphorylation and nuclear translocation of NFATs, particularly NFATc1-c4 (49). It is well established that ligand binding of RTKs and GPCRs leads to activation of PLCγs and PLCβs, respectively, resulting in IP3 production and intracellular Ca^{2+} release (50,51). In addition, many studies have reported that VEGFA activates PLCγ1 very acutely in ECs (52,53). Therefore, we questioned whether PLCγ1 has any role in VEGFA-induced NFATc1 activation in HRMVECs. To address this possibility, we studied a time course effect of VEGFA on PLCγ1 activation. VEGFA induced PLCγ1 activation acutely with

maximum effect at 1 min and declining thereafter (Figure S4A). Next, we tested the role of PLCγ1 in NFATc1 nuclear translocation. Depletion of PLCγ1 levels had no effect on VEGFA-induced NFATc1 translocation from the cytoplasm to the nucleus, indicating a lack of a role for PLCγ1 in NFATc1 activation by VEGFA (Figure S4B–D). Then, we tested the role of PLCβs in VEGFA-induced intracellular Ca^{2+} release and NFATc1 activation. First, the time course study revealed that VEGFA had no effect on the steady state levels of PLCβ1, PLCβ2, PLCβ3, or PLCβ4 in HRMVECs (Figure 7A). Second, since PLCβ1 and PLCβ3 are abundantly present in ECs, we measured their activities in response to VEGFA. Interestingly, VEGFA induced PLCβ3 but not PLCβ1 activity in a time-dependent manner in HRMVECs (Figure 7B). Third, as activation of PLCs leads to intracellular Ca^{2+} release (50,51), we next tested the effect of VEGFA on intracellular Ca^{2+} release. We found that VEGFA induces intracellular Ca^{2+} release in a time dependent manner and that this effect was substantially reduced by PLCβ3 depletion in HRMVECs (Figure 7C). Based on these findings, we next tested the role of PLCβ3 on VEGFA-induced NFATc1 nuclear translocation, proliferation, migration, sprouting, and tube formation of HRMVECs. Depletion of PLCβ3 levels blunted VEGFA-induced nuclear translocation of NFATc1, proliferation, migration, sprouting and tube formation of HRMVECs (Figure 7D–I). These observations demonstrate that PLCβ3 acts upstream to NFATc1 in mediating VEGFA-induced HRMVEC angiogenic events. In view of these in vitro findings, we also tested the role of PLCβ3 in OIR-induced CDC6 expression and retinal neovascularization using two approaches. In the first approach, we depleted PLCβ3 levels in the mouse pups' retinas by its siRNA and tested its role in OIR-induced CDC6 expression and retinal neovascularization. As expected, OIR induced CDC6 expression in the mouse pups' retinas and siRNA-mediated depletion of PLCβ3 levels completely blunted this effect (Figure S5A). Furthermore, depletion of PLCβ3 levels attenuated OIR-induced retinal neovascularization, retinal EC proliferation, and tufts and filopodia formation leading to increased avascular area (Figure S5B–E). In another approach, we used PLCβ3 global knockout mice. First, we tested the effect of genetic deletion of PLCβ3 on OIR-induced CDC6 expression in mouse pups' retinas. OIR induced CDC6 expression as compared to normoxia in the retinal ECs of WT mice (Figure 8A & B). However, OIR had little or no effect on CDC6 expression in the retinal ECs of PLCβ3 knock out mice pups (Figure 8A & B). Consistent with these observations, genetic deletion of PLCβ3 also reduced retinal neovascularization, retinal EC proliferation, and tufts and filopodia formation leading to decreased avascular area as compared to WT mice pups (Figure 8C–F). Besides these observations, retroviral-mediated overexpression of CDC6 in PLCβ3-depleted HRMVECs while alone enhancing proliferation, migration and sprouting of these cells rescued the capacity of VEGFA in triggering these angiogenic events from inhibition by PLCβ3 depletion (Figure S6A–C). Similarly, retroviral-mediated overexpression of CDC6 in the retinas of PLCβ3$^{-/-}$ mice pups restored OIR-induced retinal neovascularization from inhibition (Figure S7A–D). These results indicate that PLCβ3-dependent NFATc1-mediated CDC6 expression plays a crucial role in OIR-induced retinal neovascularization.

DISCUSSION

Diabetes, a metabolic disorder, is one of the fastest-growing health challenges of the 21st century. Data published by International Diabetes Federation (IDF) indicated that the worldwide total of adults aged 20–79 years with diabetes is 463 million, and diabetic individuals under the age of 20 total 1.1 million (54). In the past 20 years, the number of adults living with diabetes tripled, and IDF estimated that there will be 578 million adults with diabetes by 2030 and 700 million by 2045. In most countries, diabetic retinopathy continues to be a leading cause of blindness (55) and may cause disability. The prevalence of diabetic retinopathy is associated with the duration of diabetes and deteriorated glycemic control, which accelerates leucocyte adherence to the retinal vascular endothelium, resulting in EC death, vascular leakage, and capillary closure (56). After a time period with diabetes, occlusion of retinal capillaries and arterioles leads to retinal ischemia and hypoxia which, depending on the severity, progresses to retinal neovascularization (6–9, 57,58) and results in “proliferative diabetic retinopathy” (PDR). PDR is characterized by neovascular growth that is prone to leakage and bleeding. Until 1948, the factor that mediates hypoxia-induced retinal neovascularization was unknown and was termed “Factor X” (59). It took almost 50 years of research to identify Factor X as VEGF (60) and to demonstrate its major role in mediating active intraocular neovascularization in patients with ischemic retinal diseases including PDR (5,61). Several anti-VEGF drugs have been used for treating PDR (62), but these therapies are effective only in ~60% of patients (15,16, 63). In addition, these therapies caused side effects that included a transient increase in intraocular pressure and subsequent development of floaters (64). Together, the long-term use of anti-VEGF therapies may lead to tractional retinal detachment in the setting of pre-existing membranes, which is a severe vision-threatening complication (17,65). Therefore, it is essential to find alternative target molecules to treat PDR.

To this end, our results demonstrate for the first time that CDC6, a protein that is essential for DNA replication (30), plays a crucial role in OIR-induced retinal neovascularization. In validating the full blown role of CDC6 in angiogenesis, we found that CDC6 which was expressed abundantly in vasculature developing P6 retina and decreased as retinal vasculature developed, disappears in hyperoxic retinas with vessel loss and upregulates robustly in the post-OIR retinas. These findings indicate that CDC6 is involved in both developmental as well as reparative angiogenesis. It is also noteworthy that CDC6 expression levels were correlated with HIF1α levels. The expression pattern of both HIF1α and CDC6 during retinal vasculature development, during hyperoxia-mediated vessel regression and post-OIR-mediated neovascularization also point out the applicability of the OIR model to study the pathophysiology of hypoxia-induced vascular diseases. Intravitreal injection of CDC6 siRNA not only blocked VEGFA-induced proliferation, migration, sprouting, and tube formation of HRMVECs in vitro but also suppressed OIR-induced retinal neovascularization. Since downregulation of CDC6 suppresses VEGFA-induced EC angiogenic events such as EC proliferation, migration, sprouting, and tube formation, it appears that CDC6 is a major contributor of VEGFA-induced retinal neovascularization. EC proliferation is one of the essential requirements for the development of new blood vessels (66). In this regard, due to its indispensable role in DNA replication (30), CDC6 could

be involved in retinal neovascularization triggered not only by VEGFA but also by other factors that induce EC proliferation. A role for CDC6 in angiogenesis, particularly tumor angiogenesis, has also been reported previously (67). Besides its role in DNA replication, CDC6 has been shown to be involved in regulating tumor cell migration, although the underlying mechanisms were not clear (31–33). In this regard, we found that downregulation of CDC6 levels by its siRNA inhibits VEGFA-induced EC migration. Podosomes are needed to establish localized anchorages in cell-matrix contacts, thereby stabilizing cell protrusions that facilitate directional movement of the cell (41,46–47). Accordingly, a reduction in podosome numbers in CDC6-downregulated ECs suggests that CDC6 plays a role in VEGFA-induced podosome formation. Previous studies have reported that podosomes consist of an F-actin rich core which is comprised of a subset of actin-regulatory proteins including cortactin (47,48). Furthermore, it was shown that tyrosine phosphorylation of cortactin is required for actin polymerization and podosome formation (48). In view of these observations, we found that VEGFA stimulates a complex formation between cortactin and CDC6 and that phosphorylation of cortactin at Y470 residue is required for their interaction. Moreover, blocking CDC6 and cortactin interactions by overexpressing cortactin Y470F mutant attenuated VEGFA-induced podosome formation. A large body of literature suggests that VEGFA stimulates Src activation (68). Since cortactin phosphorylation at Y470 is required for its interaction with CDC6 in VEGFA-induced podosome formation, it is possible that a member of the Src family or other non-receptor tyrosine kinases such as Pyk2 might be involved in VEGFA-induced cortactin tyrosine phosphorylation and its interaction with CDC6. These findings suggest that CDC6, by interacting with cortactin and forming podosomes, plays a role in VEGFA-induced EC migration.

Previously we reported that NFATc1 mediates thrombin-induced CDC6 expression in modulating smooth muscle cell proliferation during vascular wall remodeling (45). In addition, a few studies have shown that NFATs by enhancing the expression of genes such as CXCR7, RND1 and COX2 play a role in the modulation of angiogenesis (27–29). Our findings reveal that downregulation of NFATc1 blocks both VEGFA and OIR-induced CDC6 expression in ECs. The findings that downregulation of CDC6 levels suppressed retinal neovascularization and that its expression was dependent on NATc1 activation clearly infers that NFATc1 also plays a role in VEGFA/OIR-induced retinal neovascularization. Indeed, the involvement of NFATc1 in retinal neovascularization can be supported by the observations that siRNA-mediated downregulation of NFATc1 levels in WT mice or EC-specific NFATc1 knockout blunted OIR-induced retinal EC proliferation, filopodia formation, and neovascularization. These conclusions were also confirmed by rescue experiments where forced expression of CDC6 in NFATc1$^{i\Delta EC}$ MRMVECs restored VEGFA-induced EC angiogenic responses such as migration, sprouting and tube formation. Similarly, overexpression of CDC6 in NFATc1$^{i\Delta EC}$ mice rescued OIR-induced retinal neovascularization. Together, these observations clearly show that NFATc1-mediated CDC6 expression is required for both VEGFA and OIR-induced EC angiogenic responses. Other studies have also reported that VEGFA-induced mouse retinal microvascular EC proliferation and migration requires NFAT activation, although the mechanisms were not clear (28,69).

Given the striking role of NFATc1 upstream to CDC6's induction in mediating pathological retinal neovascularization, we sought to identify the signaling mechanisms that activate NFATc1 in regulating EC angiogenic potential. Since calcineurin, a Ca^{2+}-regulated phosphatase, via dephosphorylation activates NFATc1 (70) and VEGFA activates PLCγ1 downstream to VEGFR2 (25), we examined its role in VEGFA-induced NFATc1 activation. Although VEGFA stimulated PLCγ1 phosphorylation very acutely, downregulation of PLCγ1 had no effect on VEGFA-induced NFATc1 activation. Alternatively, we found that VEGFA activates PLCβ3 in a sustained manner and that depletion of its levels reduces VEGFA-induced intracellular calcium release and NFATc1 activation. These observations show that PLCβ3 but not PLCγ1-mediated calcium release is required for NFATc1 nuclear translocation/activation by VEGFA. Furthermore, downregulation of PLCβ3 levels or deletion of PLCβ3 gene reduced OIR-induced CDC6 expression as well as retinal neovascularization. In line with our observations, Ha et al reported that silencing of PLCβ3 in human umbilical vein ECs delayed their proliferation, migration, and capillary-like tube formation (71). Also, mice lacking PLCβ3 showed reduced retinal angiogenesis with impaired endothelial proliferation and vessel formation (71). It is noteworthy that in response to hypoxia the avascular area is significantly decreased in PLCβ3$^{-/-}$ mice pups as compared to WT mice pups. It is possible that the genetic loss of PLCβ3 may be triggering activation of compensatory mechanisms leading to normalization of vasculature pattern and thereby causing decreased avascular area in response to hypoxia. Mostly the RTK agonists activate PLCγs and GPCR agonists activate PLCβs (50,51). However, our results showed that VEGFA, via its receptor VEGFR2, activates both PLCγ1 and PLCβ3, the former more acutely and the latter in a sustained manner and that PLCβ3 but not PLCγ1 is required for NFATc1 activation and CDC6 expression in modulating VEGFA/OIR-induced retinal neovascularization. Based on these novel observations, it is possible that VEGFA, via its receptor VEGFR2, may activate G proteins as well. Indeed, a recent study showed that VEGFA stimulates Gq/11 in regulating EC migration (72). In view of these observations, it is possible that VEGFA/VEGFR2 via Gq/11-PLCβ3 might be stimulating NFATc1 in the induction of CDC6 expression and retinal neovascularization. The rescue effects of retroviral-mediated overexpression of CDC6 on VEGFA-induced angiogenic responses in PLCβ3 or NFATc1-depleted HRMVECs in vitro and OIR-mediated retinal neovascularization in PLCβ3$^{-/-}$ or EC-specific NFATc1 knockout mice in vivo also support this view. Many recent studies have reported that metabolic insufficiency and/or communication between photoreceptors, microglia and EC could trigger retinal neovascualization (73,74). Since OIR model comprises of two phases; with vessel regression during the first phase (hyperoxia) and burst of new blood vessels formation during the second phase (hyeroxia-derived hypoxia), it is quite possible that the vessel loss caused by hyperoxia may lead to nutritional insufficiency in the surrounding tissue/cells, which in turn, via producing cytokines could enhance angiogenic signaling events including the expression CDC6 in ECs. Although, based on our in vitro findings in HRMVECs we presume that VEGFA could be involved in such a circuit, a possible involvement for other molecules can not be ruled out. Much effort has been directed toward pharmacological targeting of VEGF and its receptors over the past many decades in treating vascular ocular diseases, but their uses against these diseases are limited (75). Since CDC6 is essential for DNA replication and the fact that it is also involved in EC migration, sprouting,

and tube formation, targeting CDC6 may be more beneficial for inhibiting pathological retinal neovascularization and restoring normal vasculature in the ischemic retina than anti-VEGF therapies. However, lack of availability of CDC6 floxed mice is a limiting factor in determining its endothelial-specificity in the contribution of retinal neovascularization and thus awaits further investigation.

CONCLUSIONS

As depicted in Figure 8G, the above observations suggest that PLCβ3-mediated NFATc1 activation and CDC6 expression play a crucial role in retinal neovascularization. Therefore, CDC6 could be a novel target for development of therapeutics targeting pathological retinal angiogenesis.

Supplementary Material

Refer to Web version on PubMed Central for supplementary material.

ACKNOWLEDGEMENTS

We are thankful to Dr. Nathan G. Tipton for editing the manuscript.

SOURCE OF FUNDING

This work was funded by a grant EY04856 from NIH to GNR.

NONSTANDARD ABBREVIATIONS AND ACRONYMS

CDC6	cell division cycle 6
HIF1α	hypoxia inducible factor 1α
HRMVEC	human retinal microvascular endothelial cells
MCM	minichromosomal maintenance
MRMVEC	mouse retinal microvascular endothelial cells
NFAT	nuclear factor of activated T cells
OIR	oxygen-induced retinopathy
PDR	proliferative diabetic retinopathy
PLCβ3	phospholipase Cβ3
pRC	pre-replicative complex
WT	wild type
VEGFA	vascular endothelial growth factor A
VEGFR	vascular endothelial growth factor receptor

REFERENCES

1. Yau JW, Rogers SL, Kawasaki R, et al. Meta-Analysis for Eye Disease (META-EYE) Study Group. Global prevalence and major risk factors of diabetic retinopathy. Diabetes Care. 2012;35:556–564. [PubMed: 22301125]
2. World report on vision. Geneva: World Health Organization; 2019. Licence: CC BY-NC-SA 3.0 IGO. https://www.who.int/publications/i/item/9789241516570.
3. Solomon SD, Chew E, Duh EJ, Sobrin L, Sun JK, VanderBeek BL, Wykoff CC, Gardner TW. Diabetic Retinopathy: A Position Statement by the American Diabetes Association. Diabetes Care. 2017;40:412–418. [PubMed: 28223445]
4. Sun G, Zhang X, Shen YI, Sebastian R, Dickinson LE, Fox-Talbot K, Reinblatt M, Steenbergen C, Harmon JW, Gerecht S. Dextran hydrogel scaffolds enhance angiogenic responses and promote complete skin regeneration during burn wound healing. Proc Natl Acad Sci U S A. 2011;108:20976–20981.
5. Aiello LP, Pierce EA, Foley ED, Takagi H, Chen H, Riddle L, Ferrara N, King GL, Smith LE. Suppression of retinal neovascularization in vivo by inhibition of vascular endothelial growth factor (VEGF) using soluble VEGF-receptor chimeric proteins. Proc Natl Acad Sci U S A. 1995;92:10457–10461.
6. Puro DG, Kohmoto R, Fujita Y, Gardner TW, Padovani-Claudio DA. Bioelectric impact of pathological angiogenesis on vascular function. Proc Natl Acad Sci U S A. 2016;113:9934–9939. [PubMed: 27551068]
7. Marjon PL, Bobrovnikova-Marjon EV, Abcouwer SF. Expression of the pro-angiogenic factors vascular endothelial growth factor and interleukin-8/CXCL8 by human breast carcinomas is responsive to nutrient deprivation and endoplasmic reticulum stress. Mol Cancer. 2004;3:4. [PubMed: 14738568]
8. Gariano RF, Gardner TW. Retinal angiogenesis in development and disease. Nature. 2005;438:960–966. [PubMed: 16355161]
9. Krock BL, Skuli N, Simon MC. Hypoxia-induced angiogenesis: good and evil. Genes Cancer. 2011;2:1117–1133. [PubMed: 22866203]
10. Andreoli CM, Miller JW. Anti-vascular endothelial growth factor therapy for ocular neovascular disease. Curr Opin Ophthalmol. 2007;18:502–508. [PubMed: 18163003]
11. Chen J, Smith LE. Retinopathy of prematurity. Angiogenesis. 2007;10:133–140. [PubMed: 17332988]
12. Ferrara N, Kerbel RS. Angiogenesis as a therapeutic target. Nature. 2005; 438:967–974. [PubMed: 16355214]
13. Hurwitz H, Fehrenbacher L, Novotny W, Cartwright T, Hainsworth J, Heim W, Berlin J, Baron A, Griffing S, Holmgren E, Ferrara N, Fyfe G, Rogers B, Ross R, Kabbinavar F. Bevacizumab plus irinotecan, fluorouracil, and leucovorin for metastatic colorectal cancer. N Engl J Med. 2004;350:2335–2342. [PubMed: 15175435]
14. Gragoudas ES, Adamis AP, Cunningham ET Jr, Feinsod M, Guyer DR; VEGF Inhibition Study in Ocular Neovascularization Clinical Trial Group. Pegaptanib for neovascular age-related macular degeneration. N Engl J Med. 2004;351:2805–2816. [PubMed: 15625332]
15. Gasperini JL, Fawzi AA, Khondkaryan A, Lam L, Chong LP, Eliott D, Walsh AC, Hwang J, Sadda SR. Bevacizumab and ranibizumab tachyphylaxis in the treatment of choroidal neovascularisation. Br J Ophthalmol. 2012;96:14–20. [PubMed: 21791509]
16. Usui-Ouchi A, Friedlander M. Anti-VEGF therapy: higher potency and long-lasting antagonism are not necessarily better. J Clin Invest. 2019;129:3032–3034. [PubMed: 31232702]
17. Jiao C, Eliott D, Spee C, He S, Wang K, Mullins RF, Hinton DR, Sohn EH. APOPTOSIS AND ANGIOFIBROSIS IN DIABETIC TRACTIONAL MEMBRANES AFTER VASCULAR ENDOTHELIAL GROWTH FACTOR INHIBITION: Results of a Prospective Trial. Report No. 2. Retina. 2019;39:265–273. [PubMed: 29190236]
18. Arevalo JF. Intravitreal bevacizumab as anti-vascular endothelial growth factor in the management of complications of proliferative diabetic retinopathy. Med Hypothesis Discov Innov Ophthalmol. 2013;2:20–24. [PubMed: 24600636]

19. Cheung N, Lam DS, Wong TY. Anti-vascular endothelial growth factor treatment for eye diseases. BMJ. 2012;344:e2970.
20. Osaadon P, Fagan XJ, Lifshitz T, Levy J. A review of anti-VEGF agents for proliferative diabetic retinopathy. Eye (Lond). 2014;28:510–20. [PubMed: 24525867]
21. Sato T, Wada K, Arahori H, Kuno N, Imoto K, Iwahashi-Shima C, Kusaka S. Serum concentrations of bevacizumab (avastin) and vascular endothelial growth factor in infants with retinopathy of prematurity. Am J Ophthalmol. 2012;153:327–333.e1.
22. De Palma M, Biziato D, Petrova TV. Microenvironmental regulation of tumour angiogenesis. Nat Rev Cancer. 2017;17:457–474. [PubMed: 28706266]
23. Graupera M, Guillermet-Guibert J, Foukas LC, Phng LK, Cain RJ, Salpekar A, Pearce W, Meek S, Millan J, Cutillas PR, Smith AJ, Ridley AJ, Ruhrberg C, Gerhardt H, Vanhaesebroeck B. Angiogenesis selectively requires the p110alpha isoform of PI3K to control endothelial cell migration. Nature. 2008;453:662–666. [PubMed: 18449193]
24. Kerr BA, West XZ, Kim YW, Zhao Y, Tischenko M, Cull RM, Phares TW, Peng XD, Bernier-Latmani J, Petrova TV, Adams RH, Hay N, Naga Prasad SV, Byzova TV. Stability and function of adult vasculature is sustained by Akt/Jagged1 signalling axis in endothelium. Nat Commun. 2016;7:10960.
25. Sase H, Watabe T, Kawasaki K, Miyazono K, Miyazawa K. VEGFR2-PLCgamma1 axis is essential for endothelial specification of VEGFR2+ vascular progenitor cells. J Cell Sci. 2009; 122:3303–3311. [PubMed: 19706681]
26. Kitamura N, Shindo M, Ohtsuka J, Nakamura A, Tanokura M, Hiroi T, Kaminuma O. Identification of novel interacting regions involving calcineurin and nuclear factor of activated T cells. FASEB J. 2020;34:3197–3208. [PubMed: 31909857]
27. Urso K, Alfranca A, Martínez-Martínez S, Escolano A, Ortega I, Rodríguez A, Redondo JM. NFATc3 regulates the transcription of genes involved in T-cell activation and angiogenesis. Blood. 2011;118:795–803. [PubMed: 21642596]
28. Xu Y, Yang B, Hu Y, Lu L, Lu X, Wang J, Shu Q, Cheng Q, Yu S, Xu F, Huang J, Liang X. Secretion of Down Syndrome Critical Region 1 Isoform 4 in Ischemic Retinal Ganglion Cells Displays Anti-Angiogenic Properties Via NFATc1-Dependent Pathway. Mol Neurobiol. 2017;54:6556–6571. [PubMed: 27734335]
29. Suehiro J, Kanki Y, Makihara C, Schadler K, Miura M, Manabe Y, Aburatani H, Kodama T, Minami T. Genome-wide approaches reveal functional vascular endothelial growth factor (VEGF)-inducible nuclear factor of activated T cells (NFAT) c1 binding to angiogenesis-related genes in the endothelium. J Biol Chem. 2014;289:29044–29059.
30. Yan Z, DeGregori J, Shohet R, Leone G, Stillman B, Nevins JR, Williams RS. Cdc6 is regulated by E2F and is essential for DNA replication in mammalian cells. Proc Natl Acad Sci U S A. 1998;95:3603–3608. [PubMed: 9520412]
31. Zhang X, Xiao D, Wang Z, Zou Y, Huang L, Lin W, Deng Q, Pan H, Zhou J, Liang C, He J. MicroRNA-26a/b regulate DNA replication licensing, tumorigenesis, and prognosis by targeting CDC6 in lung cancer. Mol Cancer Res. 2014;12:1535–1546. [PubMed: 25100863]
32. Chen S, Chen X, Xie G, He Y, Yan D, Zheng D, Li S, Fu X, Li Y, Pang X, Hu Z, Li H, Tan W, Li J. Cdc6 contributes to cisplatin-resistance by activation of ATR-Chk1 pathway in bladder cancer cells. Oncotarget. 2016;7:40362–40376.
33. Cai J, Wang H, Jiao X, Huang R, Qin Q, Zhang J, Chen H, Feng D, Tian X, Wang H. The RNA-Binding Protein HuR Confers Oxaliplatin Resistance of Colorectal Cancer By Upregulating CDC6. Mol Cancer Ther. 2019;18:1243–1254. [PubMed: 31064870]
34. Matson JP, Dumitru R, Coryell P, Baxley RM, Chen W, Twaroski K, Webber BR, Tolar J, Bielinsky AK, Purvis JE, Cook JG. Rapid DNA replication origin licensing protects stem cell pluripotency. Elife. 2017;6: e30473.
35. Naviaux RK, Costanzi E, Haas M, Verma IM. The pCL vector system: rapid production of helper-free, high-titer, recombinant retroviruses. J Virol. 1996;70:5701–5705. [PubMed: 8764092]
36. Janjanam J, Chandaka GK, Kotla S, Rao GN. PLCβ3 mediates cortactin interaction with WAVE2 in MCP1-induced actin polymerization and cell migration. Mol Biol Cell. 2015;26:4589–606. [PubMed: 26490115]

37. Janjanam J, Rao GN. Novel role of cortactin in G protein-coupled receptor agonist-induced nuclear export and degradation of p21Cip1. Sci Rep. 2016;6:28687.
38. Singh NK, Kotla S, Dyukova E, Traylor JG Jr, Orr AW, Chernoff J, Marion TN, Rao GN. Disruption of p21-activated kinase 1 gene diminishes atherosclerosis in apolipoprotein E-deficient mice. Nat Commun. 2015;6:7450. [PubMed: 26104863]
39. Huang W, Hicks SN, Sondek J, Zhang Q. A fluorogenic, small molecule reporter for mammalian phospholipase C isozymes. ACS Chem Biol. 2011;6:223–228. [PubMed: 21158426]
40. Kumar R, Mani AM, Singh NK, Rao GN. PKCθ-JunB axis via upregulation of VEGFR3 expression mediates hypoxia-induced pathological retinal neovascularization. Cell Death Dis. 2020;11:325. [PubMed: 32382040]
41. Biosse Duplan M, Zalli D, Stephens S, Zenger S, Neff L, Oelkers JM, Lai FP, Horne W, Rottner K, Baron R. Microtubule dynamic instability controls podosome patterning in osteoclasts through EB1, cortactin, and Src. Mol Cell Biol. 2014;34:16–29. [PubMed: 24144981]
42. Smith LE, Wesolowski E, McLellan A, Kostyk SK, D'Amato R, Sullivan R, D'Amore PA. Oxygen-induced retinopathy in the mouse. Invest Ophthalmol Vis Sci. 1994;35:101–111. [PubMed: 7507904]
43. Connor KM, Krah NM, Dennison RJ, Aderman CM, Chen J, Guerin KI, Sapieha P, Stahl A, Willett KL, Smith LE. Quantification of oxygen-induced retinopathy in the mouse: a model of vessel loss, vessel regrowth and pathological angiogenesis. Nat Protoc. 2009;4:1565–1573. [PubMed: 19816419]
44. Singh NK, Hansen DE 3rd, Kundumani-Sridharan V, Rao GN. Both Kdr and Flt1 play a vital role in hypoxia-induced Src-PLD1-PKCγ-cPLA(2) activation and retinal neovascularization. Blood. 2013;121:1911–1923. [PubMed: 23319572]
45. Govatati S, Pichavaram P, Janjanam J, Guo L, Virmani R, Rao GN. Myristoylation of LMCD1 Leads to Its Species-Specific Derepression of E2F1 and NFATc1 in the Modulation of CDC6 and IL-33 Expression During Development of Vascular Lesions. Arterioscler Thromb Vasc Biol. 2020; 40:1256–1274. [PubMed: 32160773]
46. Cougoule C, Le Cabec V, Poincloux R, Al Saati T, Mège JL, Tabouret G, Lowell CA, Laviolette-Malirat N, Maridonneau-Parini I. Three-dimensional migration of macrophages requires Hck for podosome organization and extracellular matrix proteolysis. Blood. 2010; 115:1444–1452. [PubMed: 19897576]
47. Albiges-Rizo C, Destaing O, Fourcade B, Planus E, Block MR. Actin machinery and mechanosensitivity in invadopodia, podosomes and focal adhesions. J Cell Sci. 2009; 122:3037–3049. [PubMed: 19692590]
48. Tehrani S, Tomasevic N, Weed S, Sakowicz R, Cooper JA. Src phosphorylation of cortactin enhances actin assembly. Proc Natl Acad Sci U S A. 2007; 104:11933–11938.
49. Timmerman LA, Clipstone NA, Ho SN, Northrop JP, Crabtree GR. Rapid shuttling of NF-AT in discrimination of Ca2+ signals and immunosuppression. Nature. 1996;383:837–840. [PubMed: 8893011]
50. Berridge MJ. Rapid accumulation of inositol trisphosphate reveals that agonists hydrolyse polyphosphoinositides instead of phosphatidylinositol. Biochem J. 1983;212:849–958. [PubMed: 6309155]
51. Zhu X, Birnbaumer L. G protein subunits and the stimulation of phospholipase C by Gs-and Gi-coupled receptors: Lack of receptor selectivity of Galpha(16) and evidence for a synergic interaction between Gbeta gamma and the alpha subunit of a receptor activated G protein. Proc Natl Acad Sci U S A. 1996; 93:2827–2831. [PubMed: 8610126]
52. McLaughlin AP, De Vries GW. Role of PLCgamma and Ca(2+) in VEGF- and FGF-induced choroidal endothelial cell proliferation. Am J Physiol Cell Physiol. 2001;281:C1448-C1456.
53. Takahashi T, Yamaguchi S, Chida K, Shibuya M. A single autophosphorylation site on KDR/Flk-1 is essential for VEGF-A-dependent activation of PLC-gamma and DNA synthesis in vascular endothelial cells. EMBO J. 2001;20:2768–2778. [PubMed: 11387210]
54. International Diabetes Federation. IDF Atlas, 9th Edition. 2019. https://diabetesatlas.org/en/sections/worldwide-toll-of-diabetes.html.

55. GBD 2019 Blindness and Vision Impairment Collaborators; Vision Loss Expert Group of the Global Burden of Disease Study. Causes of blindness and vision impairment in 2020 and trends over 30 years, and prevalence of avoidable blindness in relation to VISION 2020: the Right to Sight: an analysis for the Global Burden of Disease Study. Lancet Glob Health. 2021; (2):e144–e160. [PubMed: 33275949]
56. Johnson MW. Etiology and treatment of macular edema. Am J Ophthalmol. 2009;147:11–21.e1.
57. Ciulla TA, Amador AG, Zinman B. Diabetic retinopathy and diabetic macular edema: pathophysiology, screening, and novel therapies. Diabetes Care. 2003;26:2653–2664. [PubMed: 12941734]
58. Curtis TM, Gardiner TA, Stitt AW. Microvascular lesions of diabetic retinopathy: clues towards understanding pathogenesis? Eye (Lond). 2009;23:1496–1508. [PubMed: 19444297]
59. Michaelson IC. The mode of development of the vascular system of the retina, with some observations on its significance for certain retinal diseases. Trans Ophthalmol Soc U K. 1948;68:137–180.
60. Leung DW, Cachianes G, Kuang WJ, Goeddel DV, Ferrara N. Vascular endothelial growth factor is a secreted angiogenic mitogen. Science. 1989;246:1306–1309. [PubMed: 2479986]
61. Aiello LP, Avery RL, Arrigg PG, et al. Vascular endothelial growth factor in ocular fluid of patients with diabetic retinopathy and other retinal disorders. N Engl J Med. 1994;331:1480–1487. [PubMed: 7526212]
62. Zhao Y, Singh RP. The role of anti-vascular endothelial growth factor (anti-VEGF) in the management of proliferative diabetic retinopathy. Drugs Context. 2018;7:212532.
63. Writing Committee for the Diabetic Retinopathy Clinical Research Network, Gross JG, Glassman AR, Jampol LM, et al. Panretinal Photocoagulation vs Intravitreous Ranibizumab for Proliferative Diabetic Retinopathy: A Randomized Clinical Trial. JAMA. 2015;314:2137–2146. [PubMed: 26565927]
64. Wu L, Martínez-Castellanos MA, Quiroz-Mercado H, Arevalo JF, Berrocal MH, Farah ME, Maia M, Roca JA, Rodriguez FJ; Pan American Collaborative Retina Group (PACORES). Twelve-month safety of intravitreal injections of bevacizumab (Avastin): results of the Pan-American Collaborative Retina Study Group (PACORES). Graefes Arch Clin Exp Ophthalmol. 2008;246:81–87. [PubMed: 17674014]
65. Ip MS, Domalpally A, Sun JK, Ehrlich JS. Long-term effects of therapy with ranibizumab on diabetic retinopathy severity and baseline risk factors for worsening retinopathy. Ophthalmology. 2015;122:367–374. [PubMed: 25439595]
66. Wang LJ, Xiao F, Kong LM, Wang DN, Li HY, Wei YG, Tan C, Zhao H, Zhang T, Cao GQ, Zhang K, Wei YQ, Yang HS, Zhang W. Intermedin Enlarges the Vascular Lumen by Inducing the Quiescent Endothelial Cell Proliferation. Arterioscler Thromb Vasc Biol. 2018;38:398–413. [PubMed: 29242270]
67. Chen X, Chen S, Pei N, Mao Y, Wang S, Yan R, Bai N, Li A, Zhang Y, Du H, Chen B, Sumners C, Li J, Li H. AAV-Mediated angiotensin 1–7 overexpression inhibits tumor growth of lung cancer in vitro and in vivo. Oncotarget. 2017;8:354–363. [PubMed: 27861149]
68. Ninchoji T, Love DT, Smith RO, Hedlund M, Vestweber D, Sessa WC, Claesson-Welsh L. eNOS-induced vascular barrier disruption in retinopathy by c-Src activation and tyrosine phosphorylation of VE-cadherin. Elife. 2021;10:e64944.
69. Bretz CA, Savage S, Capozzi M, Penn JS. The role of the NFAT signaling pathway in retinal neovascularization. Invest Ophthalmol Vis Sci. 2013;54:7020–7027. [PubMed: 24052639]
70. Takayanagi H, Kim S, Koga T, Nishina H, Isshiki M, Yoshida H, Saiura A, Isobe M, Yokochi T, Inoue J, Wagner EF, Mak TW, Kodama T, Taniguchi T. Induction and activation of the transcription factor NFATc1 (NFAT2) integrate RANKL signaling in terminal differentiation of osteoclasts. Dev Cell. 2002;3:889–901. [PubMed: 12479813]
71. Ha JM, Baek SH, Kim YH, Jin SY, Lee HS, Kim SJ, Shin HK, Lee DH, Song SH, Kim CD, Bae SS. Regulation of retinal angiogenesis by phospholipase C-β3 signaling pathway. Exp Mol Med. 2016;48:e240. [PubMed: 27311705]

72. Zeng H, Zhao D, Mukhopadhyay D. KDR stimulates endothelial cell migration through heterotrimeric G protein Gq/11-mediated activation of a small GTPase RhoA. J Biol Chem. 2002;277:46791–56798. [PubMed: 12244099]

73. Joyal JS, Sun Y, Gantner ML, et al. Retinal lipid and glucose metabolism dictates angiogenesis through the lipid sensor Ffar1. Nat Med. 2016;22:439–445. [PubMed: 26974308]

74. Liu Z, Xu J, Ma Q, et al. Glycolysis links reciprocal activation of myeloid cells and endothelial cells in the retinal angiogenic niche. Sci Transl Med. 2020;12:eaay1371.

75. Apte RS, Chen DS, Ferrara N. VEGF in Signaling and Disease: Beyond Discovery and Development. Cell. 2019;176:1248–1264. [PubMed: 30849371]

HIGHLIGHTS

1. The role of CDC6 in retinal neovascularization is not known. To this end, we report for the first time that CDC6 plays a crucial role in retinal neovascularization.
2. In addition, we show that PLCβ3 but not PLCγ1 is involved in VEGFA-induced intracellular calcium release and NFATc1 activation in modulating retinal neovascularization.
3. Furthermore, we demonstrate that PLCβ3-NFATc1 signaling is required for VEGFA/OIR-induced CDC6 expression in mediating retinal neovascularization.

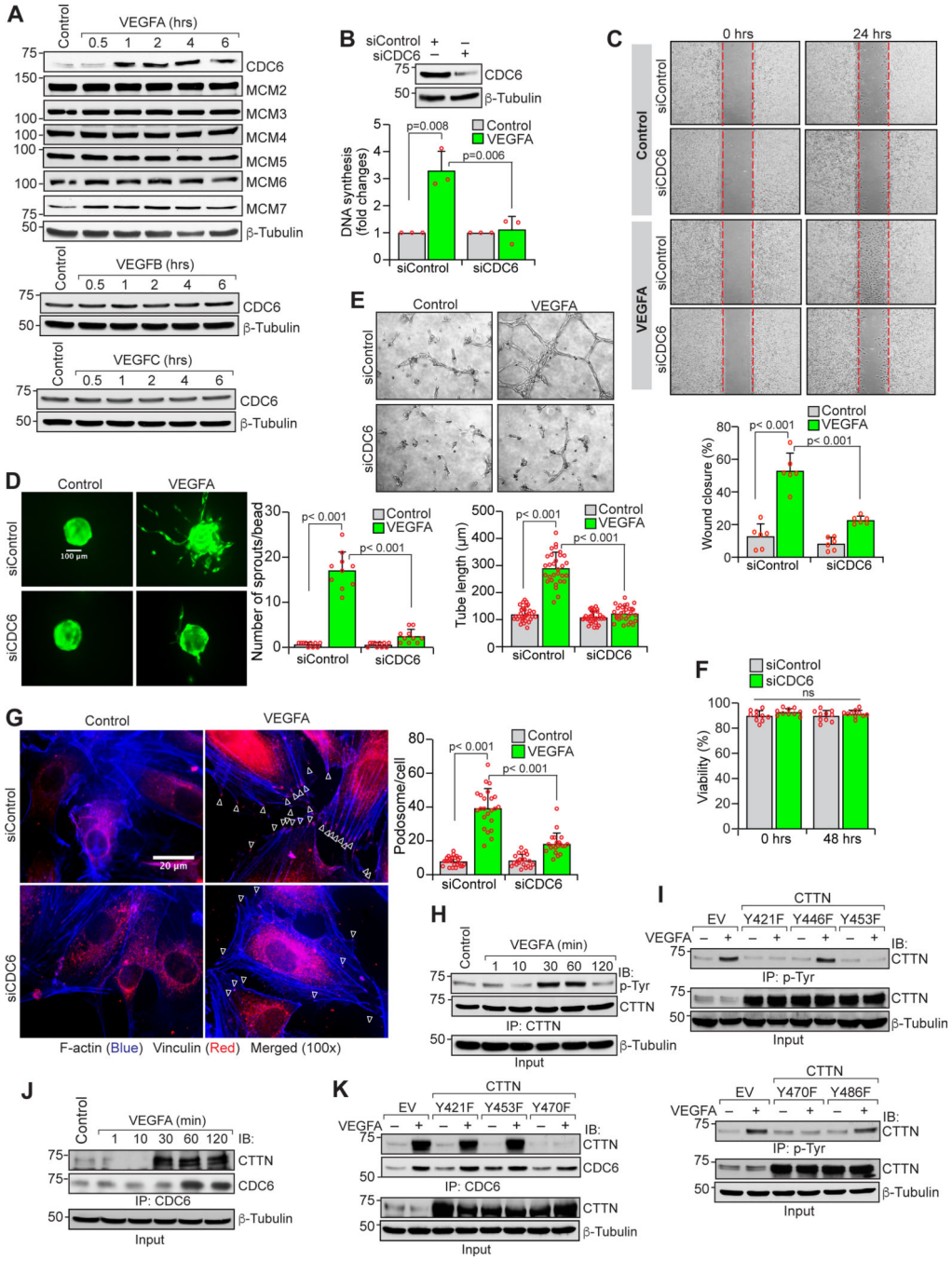

Figure 1. CDC6 mediates VEGFA-induced HRMVEC proliferation, migration, sprouting, tube formation and podosome formation.

A. Western blot analysis of control and various time periods of VEGFA, VEGFB or VEGFC-treated HRMVECs for the indicated proteins. B, Upper panel. Western blot analysis of the extracts of siControl and siCDC6-transfected HRMVECs for CDC6 and β-tubulin levels. B, Bottom panel. The effect of siControl and siCDC6 on VEGFA-induced HRMVEC DNA synthesis. C-E & G. All the conditions were the same as in bottom panel B except that cells were assayed for migration (C), sprouting (D), tube formation (E) or podosome formation (G). F. HRMVECs were transfected with siControl or siCDC6 for 6 hrs in MEM,

recovered for overnight in complete medium (EGM2), quiecced for 24 hrs in EBM2 and tested for viability as described in Materials and Methods. H. All the conditions were the same as in panel A except that equal amounts of protein from control and each treatment were immunoprecipitated (IP) with anti-cortactin antibody and the immunocomplexes were analyzed by Western blotting using antibodies against phosphotyrosine (pTyr) and the blot was then reprobed for cortactin. Input proteins were analyzed by Western blotting for β-tubulin. I. HRMVECs that were transfected with empty or the indicated tyrosine mutants of cortactin (CTTN) expressing pCMV vector and synchronized were treated with and without VEGFA for 30 min and equal amounts of protein from control and each treatment were IP with pTyr antibody and the immunocomplexes were analyzed by Western blotting using antibodies against cortactin. Input proteins were analyzed by Western blotting for cortactin and β-tubulin. J. All the conditions were the same as in panel H except that equal amounts of protein from control and each treatment were IP with anti-CDC6 antibody and immunocomplexes were analyzed by Western blotting using antibodies against cortactin and the blot was reprobed for CDC6. Input proteins were analyzed by Western blotting for β-tubulin. K. HRMVECs that were transfected with empty or the indicated tyrosine mutant cortactin (CTTN) expressing pCMV vector and synchronized were treated with and without VEGFA for 30 min and equal amounts of protein from control and each treatment were IP with anti-CDC6 antibody, the immunocomplexes were analyzed by Western blotting using antibodies against cortactin and the blot was reprobed for CDC6. Input proteins were analyzed by Western blotting for cortactin and β-tubulin. Bar graphs represent quantitative analysis. Values are presented as Mean ± SD. Scale bars in panels D and G are 100 and 20 μm, respectively.

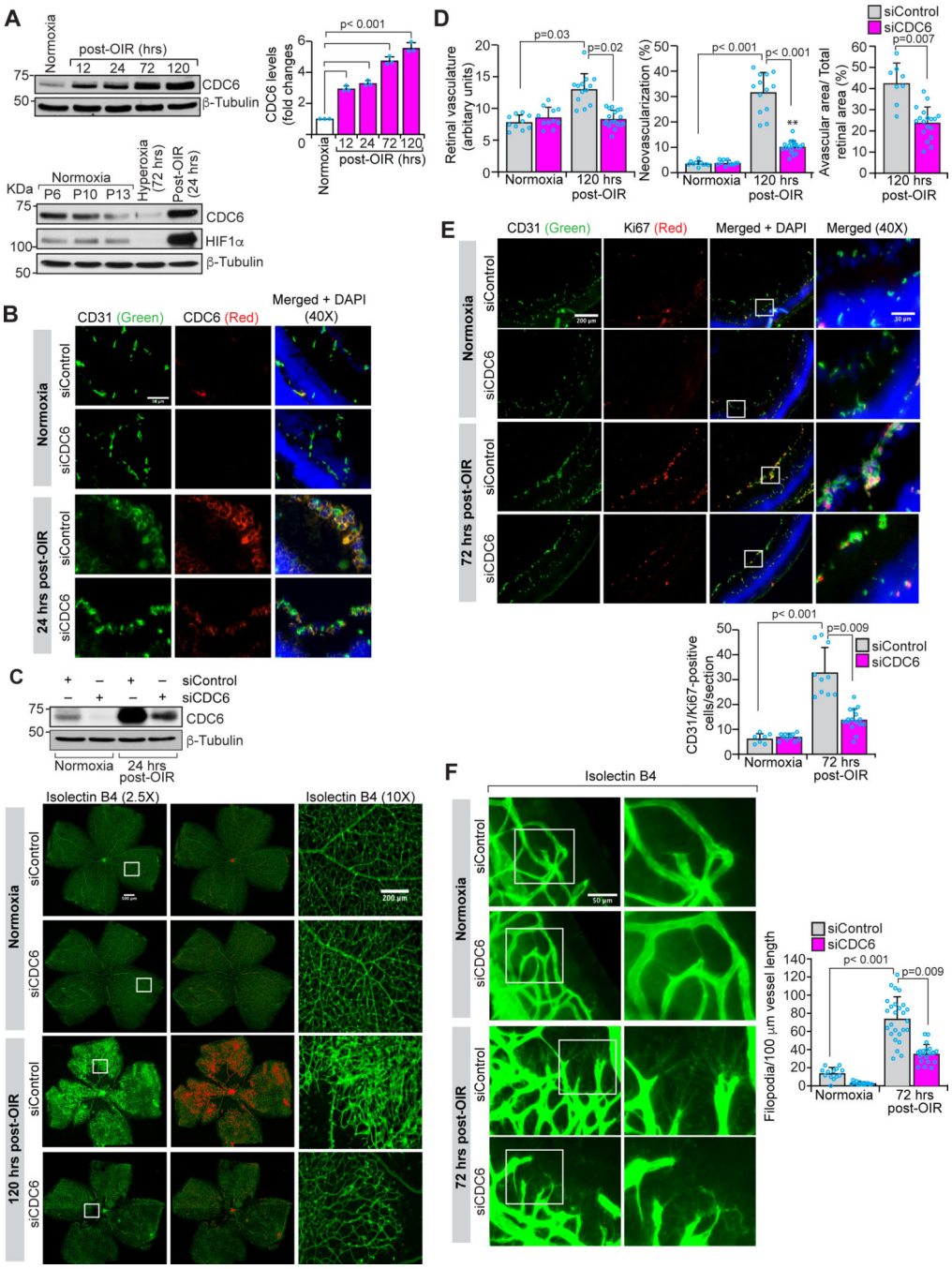

Figure 2. CDC6 mediates retinal neovascularization.

A, Upper panel. Western blot analysis of retinal extracts of normoxic and the indicated time periods of post OIR WT mice pups for CDC6 levels. The blot was reprobed for β-tubulin. Bar graph represents quantitative analysis. A, Bottom panel. Retinas were isolated from mice pups at the indicated conditions and an equal amount of protein from each retinal extract was analyzed by Western blotting for CDC6 and HIF1α levels using their specific antibodies and the blot was reprobed for β-tubulin. B. Normoxic and hyperoxic mice pups were injected intravitreally with 1 μg/0.5 μl/eye of siControl or siCDC6 at

P11 and P12 and, at 24 hrs post OIR (P13), eyes were enucleated, fixed, sections were made and coimmunostained for CD31 and CDC6 (scale bar, 50 μm). C, Upper panel. All the conditions were the same as in panel B except that at 24 hrs post OIR, eyes were enucleated and retinal extracts were prepared and analyzed by Western blotting for CDC6 and β-tubulin. C, Lower panel. All the conditions were the same as in panel B except that the pups received the indicated siRNA at P11, P12 and P13 and at 120 hrs post OIR (P17), eyes were enucleated, fixed, retinas were isolated, stained with isolectin B4 and flat mounts were prepared. Retinal vascularization is shown in the first column at 2.5X magnification (scale bar, 500 μm) and neovascularization is highlighted in red in the second column. The third column shows the selected rectangular areas of the images in the first column at 10X magnification (scale bar, 200 μm). D. Retinal vasculature, retinal neovascularization and avascular area were determined as described in “Materials and Methods” using the retinal flat mounts prepared in bottom panel C. E. Upper panel: All the conditions were the same as in bottom panel C except that at 72 hrs of post OIR (P15), eyes were enucleated, fixed, sections were made and coimmunostained for CD31 and Ki67. Retinal EC proliferation was measured by counting CD31 and Ki67-positive cells that extended anterior to the inner limiting membrane in each section and shown in the bottom bar graph. The scale bars in the far left and far right columns are 200 μm and 50 μm, respectively. F. Left panel: All the conditions were the same as in bottom panel C except that the retinal flat mounts were examined for filopodia at 40X magnification (scale bar, 50 μm). Right panel: Quantitative analysis of the number of filopodia/unit vessel length. Values are presented as Mean ± SD.

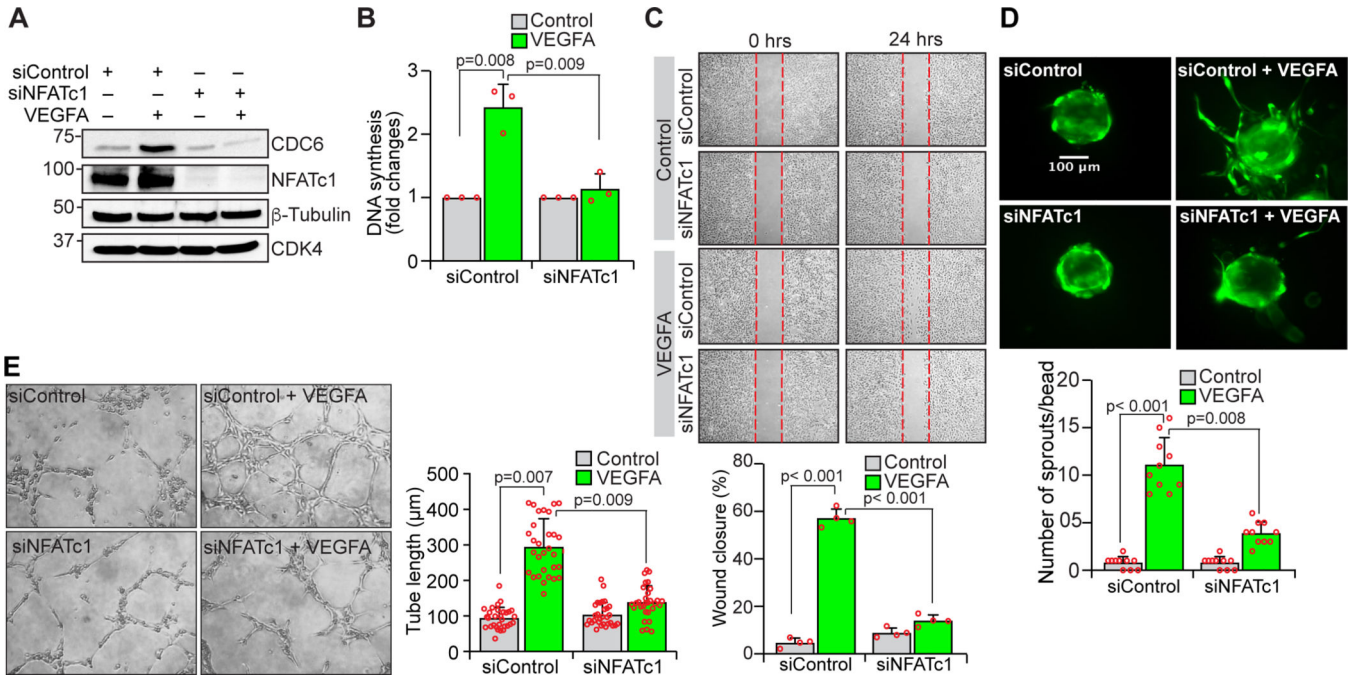

Figure 3. NFATc1 mediates VEGFA-induced CDC6 expression, HRMVEC proliferation, migration, sprouting, and tube formation.

A. The effect of siControl, siNFATc1 on VEGFA- induced (1 h) CDC6 expression in HRMVECs. The blot was sequentially reprobed for NFATc1, β-tubulin and CDK4 to show the specificity and efficacy of the siRNA on its target and off-target molecules. B-E. HRMVECs that were transfected with siControl or siNFATc1 and synchronized were tested for VEGFA-induced DNA synthesis (B), migration (C), sprouting (D) and tube formation (E). Bar graphs represent quantitative analysis. Values are presented as Mean ± SD. Scale bar in panel D is 100 μm.

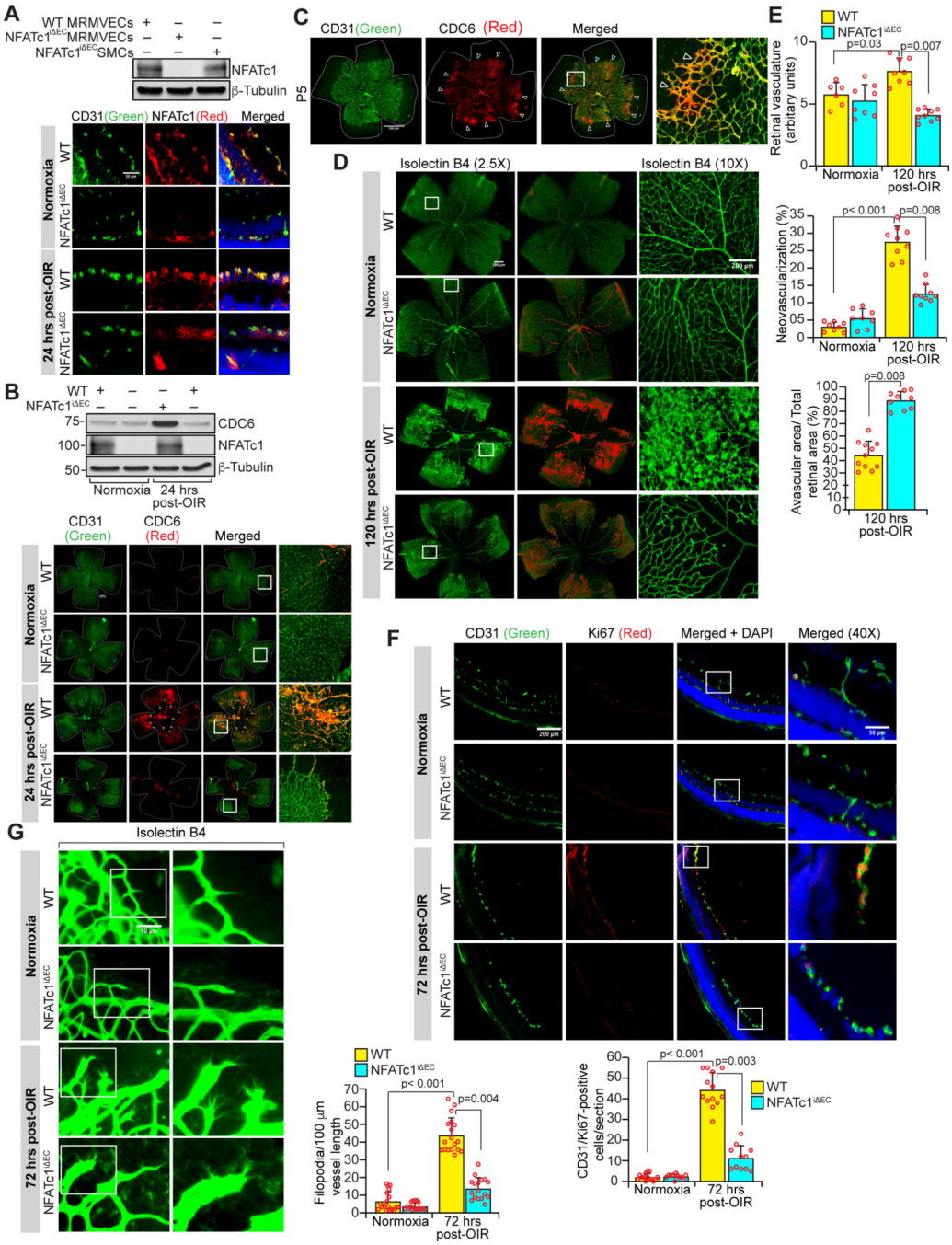

Figure 4. EC-specific knockdown of NFATc1 suppresses hypoxia-induced CDC6 expression and retinal neovascularization.

A, Uppaer panel. Retinal ECs and aortic SMCs from the indicated mice were analyzed by Western blotting for NFATc1 levels using its specific antibody and the blot was reprobed for β-tubulin. A, Bottom panel. WT and NFATc1$^{flox/flox}$:Cdh5-Cre^{ERT2} mouse pups with dams were housed in normoxia or in a hyperoxia chamber and exposed to hyperoxia (75% O_2) from P7 to P12. At P9 and P10, the normoxic and hyperoxic NFATc1$^{flox/flox}$:Cdh5-Cre^{ERT2} mice pups were injected (IP) with 100 µg of tamoxifen and the eyes from normoxic and 72 hrs post OIR pups (P15) were enucleated, fixed, sections were made and coimmunostained

for CD31 and NFATc1 (scale bar, 50 μm). B, Upper panel. All the conditions were the same as in panel A except that normoxic and 24 hrs post OIR (P13) pups' retinal extracts were prepared and analyzed by Western blotting for CDC6, NFATc1, and β-tubulin levels. B, Lower panel. All the conditions were the same as in panel A except that eyes from normoxic and 24 hrs post OIR pups were enucleated, fixed, retinas were isolated, immunostained with anti-CDC6 and anti-CD31 antibodies, and flat mounts were prepared and examined under a Zeiss inverted fluorescence microscope (Axiovision Observer.z1) (scale bar, 50 μm). The images in the extreme right column represent the digital magnification of the images shown in the immediate left column by rectangular boxes. C. Eyes from P5 mice pups were enucleated, fixed, retinas isolated, coimmunostained with anti-CDC6 and anti-CD31 antibodies, and flat mounts were prepared and examined under a zeiss inverted fluorescence microscope (Axiovision Observer.z1). Arrows in the 3rd and 4th columns indicate CDC6 expression in the vascular front (scale bar, 500 μm). D. All the conditions were the same as in panel A except that eyes were enucleated from normoxic and 120 hrs post OIR pups (P17), fixed, retinas were isolated, stained with isolectin B4, flat mounts were prepared, and retinal vascularization and neovascularization were measured. Retinal vascularization is shown in the first column at 2.5X magnification (scale bar 500 μm) and neovascularization is highlighted in red in the second column. The third column shows the selected rectangular areas of the images in the first column at 10X magnification (scale bar, 200 μm). E. Retinal vasculature, retinal neovascularization and avascular area were determined as described in "Materials and Methods" using the retinal flat mounts prepared in panel D. F. Upper panel: All the conditions were the same as in panel A except that the sections were coimmunostained for CD31 and Ki67. The extreme right column shows 40X magnification of the areas selected by rectangular boxes in the immediate left column images (scale bars in the far left and far right columns are 200 and 50 μm, respectively). Retinal EC proliferation was measured by counting CD31 and Ki67-positive cells from the inner limiting membrane to the extended region in each section and presented in the bottom bar graph. G. All the conditions were the same as in panel D except that at P15 the retinas were isolated, stained with isolectin B4, and flat mounts were prepared and examined for filopodia under fluorescent microscope at 40X magnification (scale bar, 50 μm). Bar graph on the right represents quantitative analysis. Values are presented as Mean ± SD.

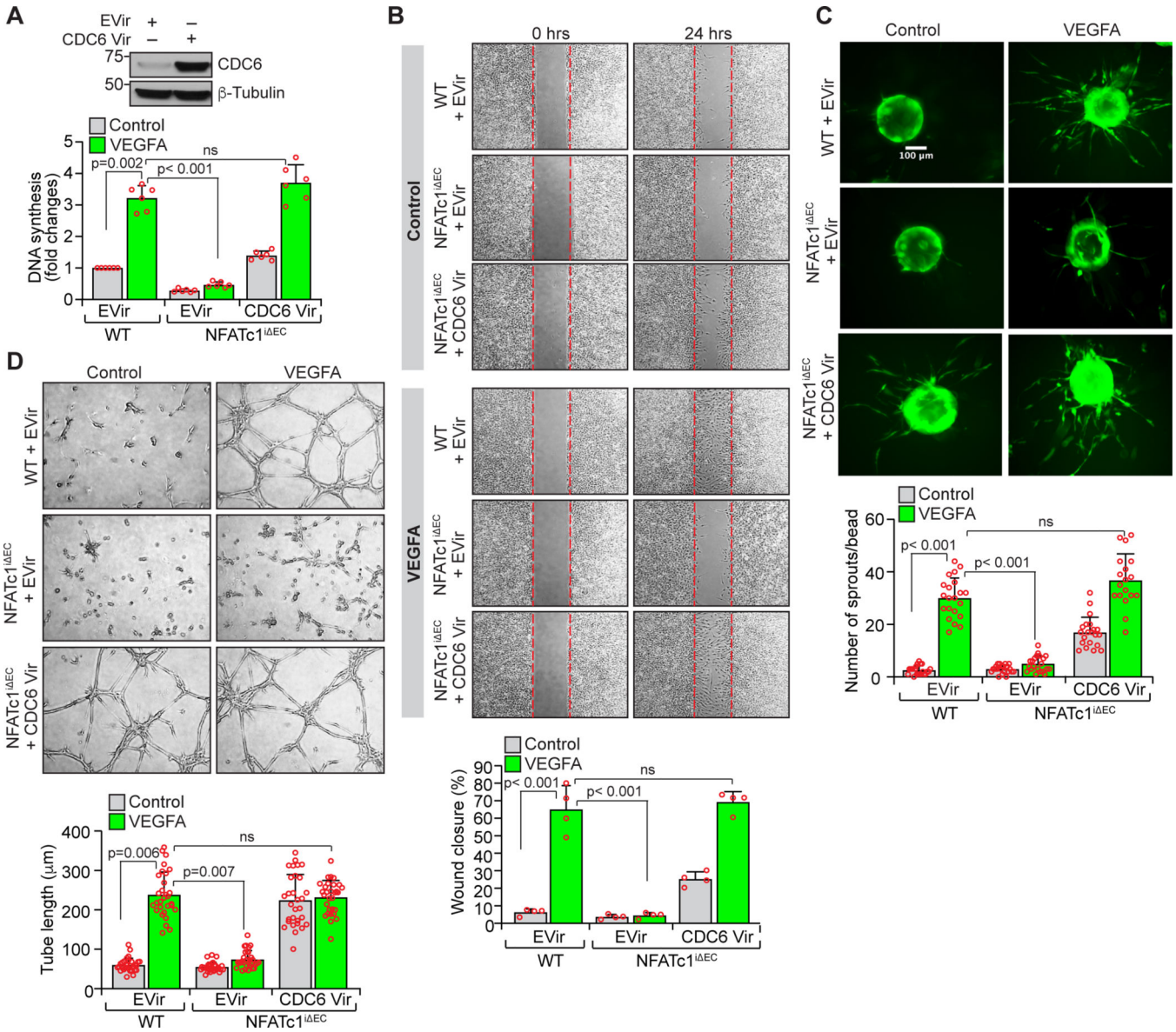

Figure 5. Forced expression of CDC6 in NFATc1$^{i\Delta EC}$ retinal ECs restores VEGFA-induced proliferation, migration, sprouting and tube formation.

A, Upper panel. MRMVECs from WT and NFATc1$^{i\Delta EC}$ mice were isolated, infected with empty or CDC6 expression retrovirus, and 36 h later cell extracts were prepared and analyzed by Western blotting for CDC6 and β-tubulin levels. A, Bottom panel. All the conditions were the same as in upper panel A except that after 24 hrs of retroviral infection, cells were synchronized for 24 hrs and subjected to VEGFA-induced DNA synthesis. B-D. All the conditions were the same as in bottom panel A except that cells were subjected to VEGFA-induced migration (B), sprouting (C) and tube formation (D). Bar graphs represent quantitative analysis. Values are presented as Mean ± SD. Scale bar in panel C is 100 μm.

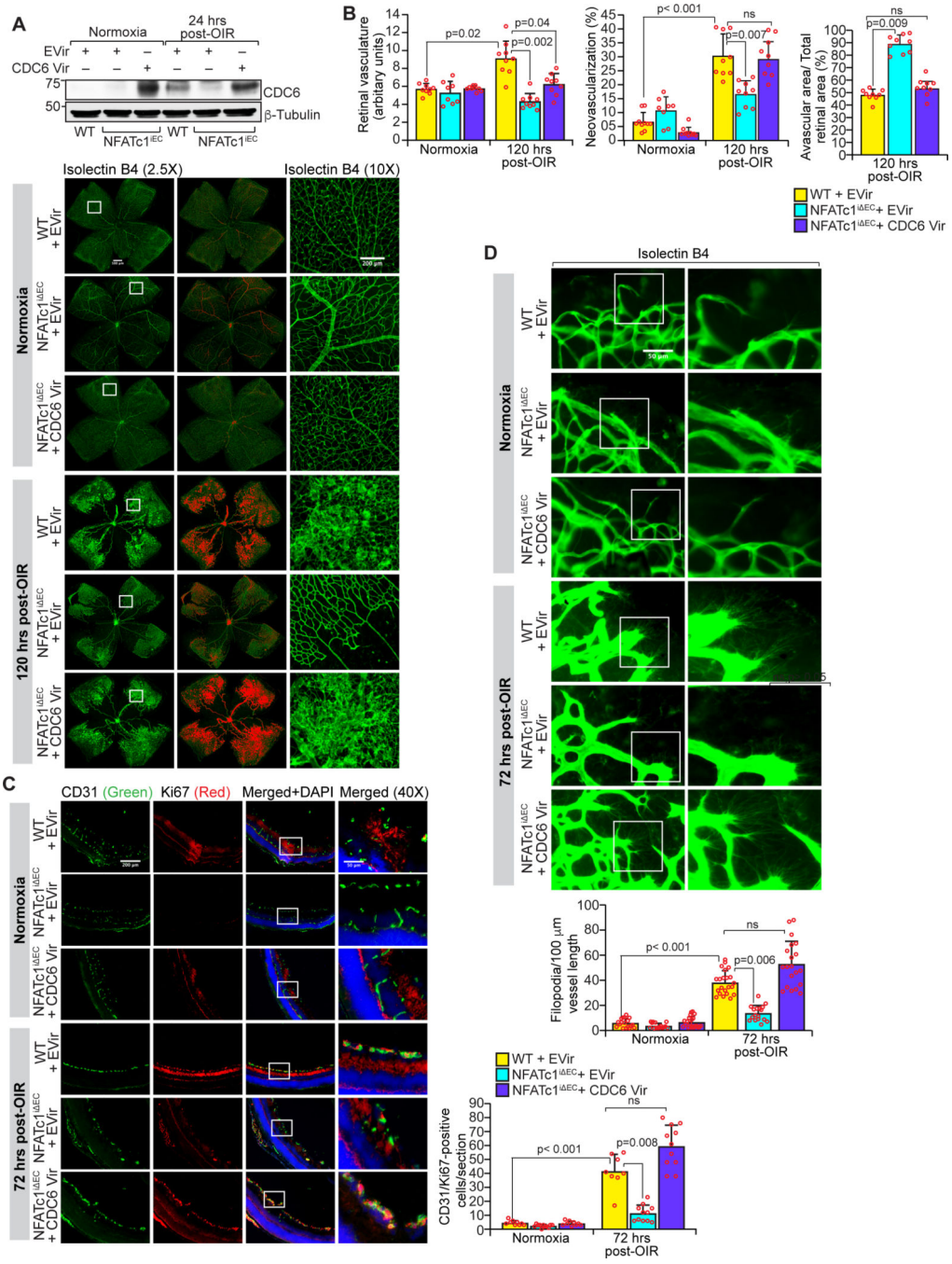

Figure 6. Forced expression of CDC6 in NFATc1$^{i\Delta EC}$ mice pups' retina restores hypoxia-induced retinal neovascularization.

A, Upper panel. WT and NFATc1$^{flox/flox}$:Cdh5-Cre^{ERT2} mice pups with dams were housed in normoxia or in a hyperoxia chamber and exposed to hyperoxia from P7 to P12. At P9 and P10, the normoxic or hyperoxic NFATc1$^{flox/flox}$:Cdh5-Cre^{ERT2} mice pups were injected (IP) with 100 μg tamoxifen. Then, at P10 and P11, WT mice pups received with 40 moi/0.5 μl/eye of empty retrovirus whereas NFATc1$^{flox/flox}$:Cdh5-Cre^{ERT2} mice pups received with 40 moi/0.5 μl/eye of empty or CDC6 expression retrovirus intravitreally. At 24 hrs post OIR (P13), retinal extracts were prepared and analyzed by Western blotting for CDC6 and β-

tubulin. Bottom panel. All the conditions were the same as in the upper panel A except that at 120 hrs post OIR (P17), eyes were enucleated, fixed, retinas were isolated, stained with isolectin B4, and flat mounts were prepared and examined under a fluorescent microscope for retinal neovascularization. Retinal vascularization is shown in the first column (scale bar, 500 μm). Neovascularization is highlighted in red in the second column. The third column shows the selected rectangular areas of the images in the first column under 10X magnification (scale bar, 200 μm). B. Retinal vasculature, neovascularization and avascular area were determined as described in the "Materials and Methods" using the retinal flat mounts prepared in bottom panel A. C. All the conditions were the same as in bottom panel A except that at 72 hrs post OIR (P15), eyes were enucleated, fixed and cross-sections were made and coimmunostained for CD31 and Ki67. The right column (scale bar, 50 μm) shows the higher magnification (40X) of the areas selected by the rectangular boxes in the left column images (scale bar, 200 μm). D. All the conditions were the same as in bottom panel A except that at 72 hrs post OIR (P15), retinas were isolated, stained with isolectin B4, and flat mounts were prepared and examined for filopodia under fluorescent microscope at 40X (scale bar, 50 μm). Bar graphs represent quantitative analysis. Values represent Mean ± SD.

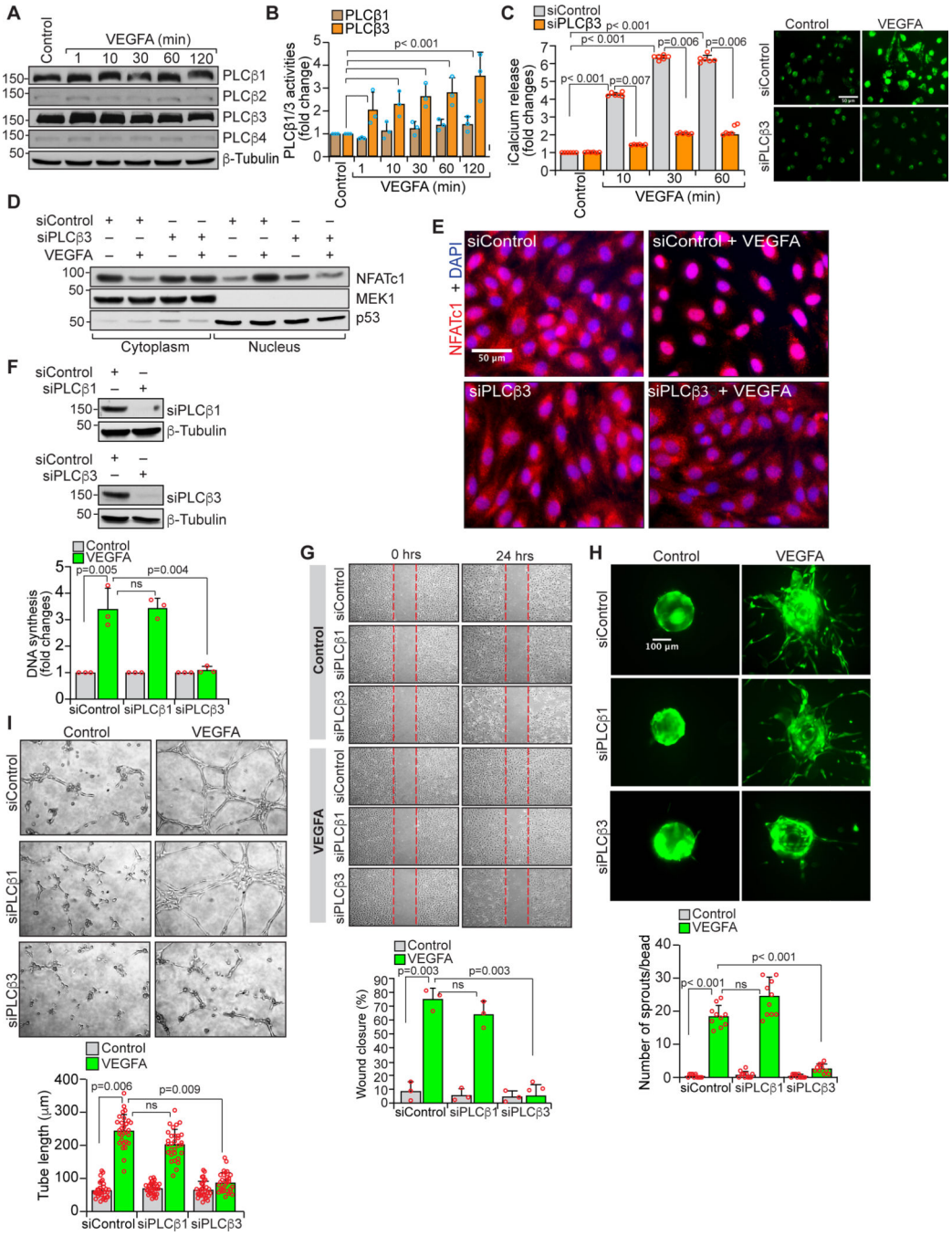

Figure 7. PLCβ3 mediates VEGFA-induced NFATc1 activation, HRMVEC proliferation, migration, sprouting and tube formation.

A. Western blot analysis of control and various time periods of VEGFA-treated HRMVECs for PLCβ1, PLCβ2, PLCβ3, and PLCβ4 levels. The blot was reprobed for β-tubulin.

B. HRMVECs were treated with or without VEGFA for the indicated time periods and assayed for PLCβ1 and PLCβ3 activities as described in Materials and Methods. C, left panel. HRMVECs were transfected with siControl or siPLCβ3, quiesced, preloaded with Fluo-8 AM and intracellular calcium release in response to VEGFA at the indicated time period was measured by flurometry. C, right panel. All the conditions were the same as

in left panel except that calcium release at 30 min of VEGFA treatment was measured by fluorescence miscroscopy. D. HRMVECs that were transfected with siControl or siPLCβ3 and synchronized were treated with and without VEGFA for 30 min and nuclear and cytoplasmic extracts were prepared and analyzed by Western blotting for NFATc1 nuclear translocation. The blot was reprobed sequentially for MEK1 and p53 levels to show the purity of the cytoplasmic and nuclear extracts, respectively. E. All the conditions were same as in panel D except that HRMVECs were immunostained with anti-NFATc1 antibody to examine NFATc1 nuclear translocation. F, Upper and middle panels. Western blot analysis showing the efficacy of siPLCβ1 and siPLCβ3 on the downregulation of PLCβ1 and PLCβ3 levels in HRMVECs. F, Bottom panel. The effect of siPLCβ1 and siPLCβ3 on VEGFA-induced HRMVEC DNA synthesis. G-I. All the conditions were the same as in bottom panel (F) except that cells were subjected to VEGFA-induced migration (G), sprouting (H) or tube formation (I). Values are presented as Mean ± SD. Scale bars in panels C (right panel), E and H are 50 μm, 50 μm and 100 μm, respectively.

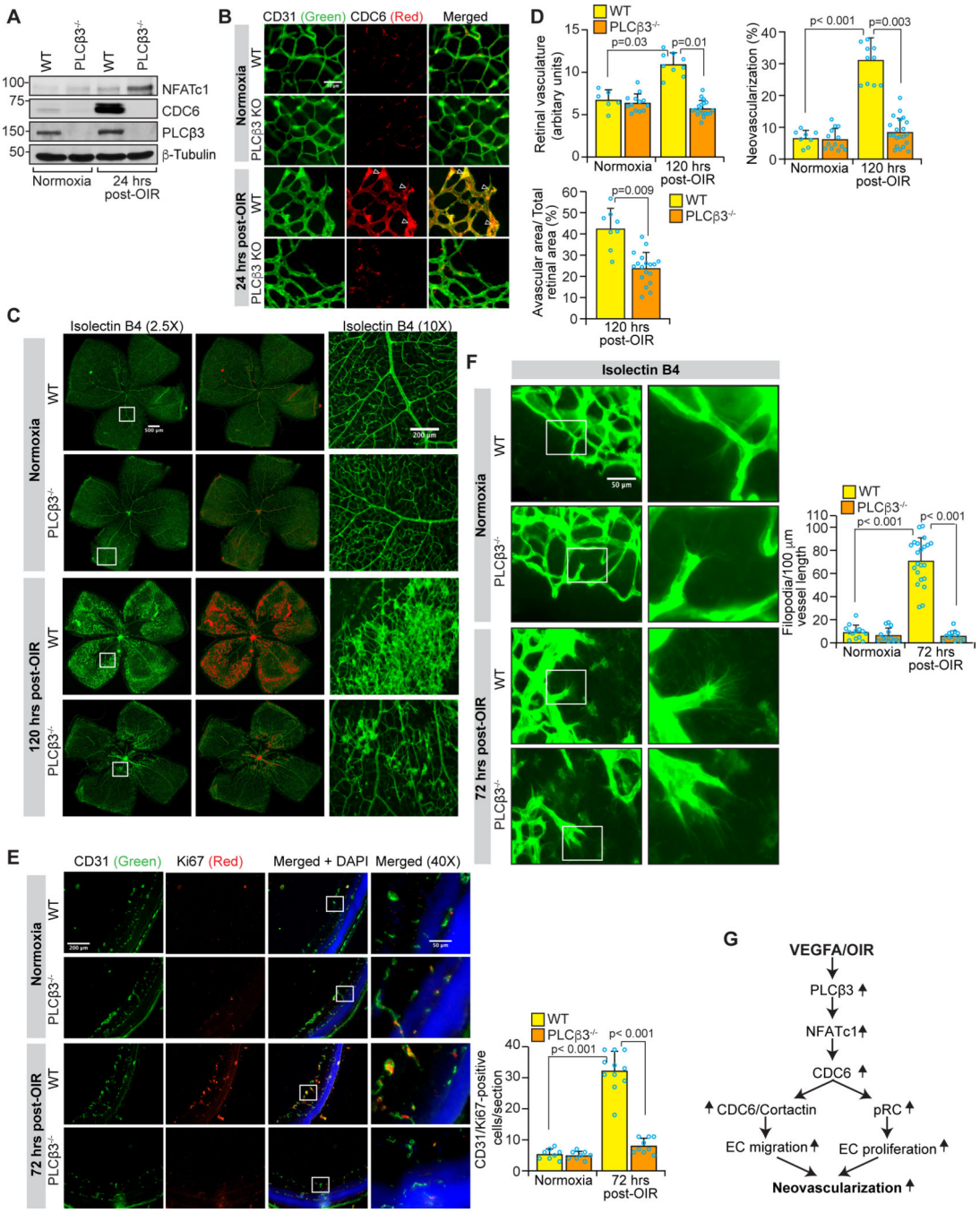

Figure 8. PLCβ3 mediates hypoxia-induced CDC6 expression and retinal neovascularization.

A. WT and PLCβ3$^{-/-}$ mice pups with dams were housed in normoxia or in a hyperoxia chamber and exposed to hyperoxia from P7 to P12. At P12 mice pups were returned to normal air to develop hyeroxia-mediated hypoxia. Normoxic or 24 hrs post OIR (P13) retinas were isolated, extracts were prepared and analyzed by Western blotting for NFATc1 and CDC6 levels. The blot was reprobed for PLCβ3 and β-tubulin. B. All the conditions were the same as in panel A except that at 24 hrs post OIR (P13), eyes were enucleated, retinas were isolated, coimmunostained for CD31 and CDC6, flat mounts were prepared

and examined under fluorescence microscope (scale bar, 50 μm). C, All the conditions were the same as in panel B except that at 120 hrs post OIR (P17), eyes were enucleated, retinas isolated, stained with isolectin B4, and flat mounts were prepared and examined under a fluorescent microscope for retinal neovascularization. Retinal vascularization is shown in the first column (scale bar, 500 μm). Neovascularization is highlighted in red in the second column. The third column shows the selected rectangular areas of the images in the first column under 10X magnification (scale bar, 200 μm). D. Retinal vasculature, neovascularization and avascular area were determined as described in the “Materials and Methods” using flat mounts prepared in panel C. E. All the conditions were the same as in panel B except that at P15, eyes from normoxic and 72 hrs post OIR pups were enucleated, fixed, cross-sections made and coimmunostained for CD31 and Ki67. The right column (scale bar, 50 μm) shows the higher magnification (40X) of the areas selected by the rectangular boxes in the left column images (scale bar, 200 μm). F. All the conditions were the same as in panel C except that at P15, eyes were enucleated, retinas isolated, stained with isolectin B4, and flat mounts were prepared and examined under a fluorescent microscope for filipodia (scale bar, 50 μm). G. Schematic diagram depicting the proposed signaling pathway of CDC6 expression mediating retinal neovascularization. Bar graphs represent quantitative analysis. Values represent Mean± S.D.